arXiv:astro-ph/0001492v1 27 Jan 2000

Mapping the Galactic Halo I. The "Spaghetti" Survey

Heather L. Morrison[1,2]

Department of Astronomy, Case Western Reserve University, Cleveland OH 44106-7215
electronic mail: heather@vegemite.astr.cwru.edu

Mario Mateo

Department of Astronomy, University of Michigan, 821 Dennison Bldg., Ann Arbor, MI 48109–1090
electronic mail: mateo@astro.lsa.umich.edu

Edward W. Olszewski

Steward Observatory, University of Arizona, Tucson, AZ 85721
electronic mail: edo@as.arizona.edu

Paul Harding

Steward Observatory, University of Arizona, Tucson, Arizona 85726
electronic mail: harding@billabong.astr.cwru.edu

R.C. Dohm-Palmer

Department of Astronomy, University of Michigan, 821 Dennison Bldg., Ann Arbor, MI 48109–1090
electronic mail: rdpalmer@astro.lsa.umich.edu

Kenneth C. Freeman

Mount Stromlo and Siding Spring Observatories, ANU, Private Bag, Weston Creek PO, 2611 Canberra, ACT, Australia
electronic mail: kcf@mso.anu.edu.au

John E. Norris

Mount Stromlo and Siding Spring Observatories, ANU, Private Bag, Weston Creek PO, 2611 Canberra, ACT, Australia
electronic mail: jen@mso.anu.edu.au

and

[1]Cottrell Scholar of Research Corporation and NSF CAREER fellow

[2]and Department of Physics

Miwa Morita

Steward Observatory, University of Arizona, Tucson, AZ 85721
electronic mail: mmorita@as.arizona.edu

ABSTRACT

We describe a major survey of the Milky Way halo designed to test for kinematic substructure caused by destruction of accreted satellites. We use the Washington photometric system to identify halo stars efficiently for spectroscopic followup. Tracers include halo giants (detectable out to more than 100 kpc), blue horizontal branch stars, halo stars near the main sequence turnoff, and the "blue metal-poor stars" of Preston et al. (1994). We demonstrate the success of our survey by showing spectra of stars we have identified in all these categories, including giants as distant as 75 kpc. We discuss the problem of identifying the most distant halo giants. In particular, extremely metal-poor halo K dwarfs are present in approximately equal numbers to the distant giants for $V > 18$, and we show that our method will distinguish reliably between these two groups of metal-poor stars.

We plan to survey 100 square degrees at high galactic latitude, and expect to increase the numbers of known halo giants, BHB stars and turnoff stars by more than an order of magnitude. In addition to the strong test that this large sample will provide for the question "was the Milky Way halo accreted from satellite galaxies?", we will improve the accuracy of mass measurements of the Milky Way beyond 50 kpc via the kinematics of the many distant giants and BHB stars we will find.

We show that one of our first datasets constrains the halo density law over galactocentric radii of 5–20 kpc and z heights of 2–15 kpc. The data support a flattened power-law halo with b/a of 0.6 and exponent –3.0. More complex models with a varying axial ratio may be needed with a larger dataset.

Subject headings: Galaxy: evolution — Galaxy: formation — Galaxy: halo — Galaxy: stellar content

1. INTRODUCTION

How much of the Galaxy's halo was accreted from satellite galaxies? What fraction of these accretions have left substructure that we can detect today? Hierarchial galaxy formation pictures (Davis et al. 1985; Governato et al. 1997; Klypin et al. 1999) suggest that structure forms first in small clumps which later combine to make larger galaxies. While this picture describes dark matter rather than stars, it is reasonable to expect that some stars would have formed in these dense clumps of matter at early times. This is borne out by the fact that almost all of the Local

Group dwarf galaxies contain stars with ages greater than 10 Gyr (Mateo 1998). In studies of the Milky Way, the first suggestion that the Galaxy's halo did not form in a fast, uniform collapse (Eggen et al. 1962) was made by Searle and Zinn (1978), who noted that the horizontal-branch morphology of the outer halo globulars could be explained by a younger mean age. These clusters would have originated in "transient protogalactic fragments that continued to fall into ..... the Galaxy for some time after the collapse of its central regions".

Strong variations in the Galaxy's potential associated with the formation of the inner disk and bar, plus the shorter orbital timescales there, may have erased the kinematic signature of halo accretion in its inner regions. Substructure may persist for many Gyr further from the galactic center (Johnston et al. 1995; Harding et al. 1999). We see evidence for accretion not only in the Sgr dwarf galaxy, which is being tidally disrupted on its current passage close to the Galaxy's disk (Ibata et al. 1994), but also in the detection of various moving groups in the halo field (Majewski et al. 1994; Helmi et al. 1999). These latter objects are particularly interesting and surprising because they are at relatively small distances from the galactic center (8–10 kpc).

Figure 1(a) shows in histogram form the numbers of distant halo objects known to date. Globular clusters and dwarf spheroidal galaxies are not included. It is not surprising, with such small samples, that almost all the discoveries of halo substructure to date have been serendipitous. In this paper, we will describe a survey which will give a *quantitative* answer to the question "how much of the halo was accreted?" by identifying a sample comprising a large number of halo stars out to great distances. (Figure 1(b) shows how the situation has improved after our first spectroscopic followup run on the KPNO 4m.)

In Section 2 we discuss the design of our survey and the tracers we use, together with the region of the halo that each tracer will sample. Section 3 discusses our photometric selection technique in detail for each tracer, showing its efficacy with spectra of stars found in each category. We also discuss the possible contaminants of our sample and how we reject them. Section 4 uses the numbers of turnoff stars found by our survey in various directions to constrain the density distribution of the halo. We also report the first evidence of spatial substructure in the halo.

Future papers in this series will discuss our simulations of the breakup of satellites and their observational consequences (Harding et al. 1999), our photometric survey (Dohm-Palmer et al. 1999), our spectroscopy of distant metal-poor giants and BHB stars (Olszewski et al. 1999) and evidence for spatial substructure in our photometric data (Morrison et al. 2000).

2. SURVEY DESIGN

Because substructure is visible in velocity space long after it disappears in density space (Johnston et al. 1995; Harding et al. 1999), we aim to obtain velocity data on a large sample of halo stars. Harding et al. (1999) discuss the signature that tidally disrupting streams will show in velocity histograms: although the observed signature does depend on the viewing geometry and initial

conditions of the accretion, in many cases velocity histograms will be bimodal or multi-modal. The features that correspond to disrupted satellites will show a velocity dispersion of order tens of kilometers per second. Since substructure will survive longest in the outer Galaxy, distant halo tracers are advantageous. If we restrict our spectroscopic follow-up to 4m-class telescopes, this means that halo red giants and blue horizontal branch stars are the tracers of choice because of their intrinsic luminosity. However, these stars are intrinsically rare, and so they limit our detection methods for substructure — for example, it is impossible to find a sample of 100 halo giants in a field of size 1 deg^2. Samples of this size are needed for methods of substructure detection based on velocity histograms. In order to have more sensitivity to subtle signatures of accretion, we also need tracers which are more numerous, such as halo turnoff stars. We shall, however, not be able to probe the extreme outer halo with these less luminous stars until 8m-class telescopes are more generally available.

The stellar halo provides a very small fraction of the Milky Way's luminosity — in the solar neighborhood, the disk-to-halo star number ratio is ∼800:1, (Bahcall and Casertano 1986; Morrison 1993), and even the thick disk outnumbers the halo by ∼40:1. Thus it is important to use a method which will *efficiently* pre-select halo stars before obtaining velocities.

2.1. Sky Coverage

When aiming to answer a question about the origin of the entire halo, all-sky coverage would be ideal. Johnston et al. (1996) discuss such a survey for halo substructure, which, unfortunately, is not feasible at present. Existing all-sky surveys based on photographic plates cannot produce photometry accurate enough to efficently select halo objects apart from rare blue horizontal branch stars. Any spatial substructure in the halo will be washed out by the many foreground disk and thick disk stars in a photographic survey. The Sloan survey (Gunn 1995) plans to cover one quarter of the sky at high galactic latitude in the North. The photometry from this survey will be sufficiently accurate to enable the identification of halo turnoff stars and BHB stars, but not the rare distant red halo giants we discuss below. These stars, which will be inseparably contaminated by foreground K dwarfs in the Sloan colors, are particularly valuable for this project because they probe the extreme outer halo.

We have chosen to use a pencil-beam survey of various high-latitude fields, using CCD photometry and the Washington system to select the halo stars, and then carry out follow-up spectroscopy to search for kinematic substructure.

Even with the most extreme hypothesis that the entire halo is composed of tidal streams, their filling factor on the sky will still be small. Some fields will therefore contain more stars than the average and some considerably fewer. A large number of different pointings is preferable to maximize the chance of hitting a single stream. For example, assuming a typical dimension for a stream of 2 degrees by 100 degrees, 50 of these would cover only 25 percent of the sky. We have

chosen to survey initially 100 square degrees of the sky, in 100 different fields randomly distributed at high galactic latitude (generally above $|b| = 45$), with most fields having galactic longitude between 90 and 270.

We chose in general to stay away from the quadrants which include the galactic center for two reasons. First, structure is more readily destroyed close to the galactic center, which lowers our chance of detecting it. The best place to look for substructure is the outer halo, where dynamical times are long and tidal forces small. Thus, the galactic anticenter is better since the galactocentric radii of the stars we detect will be larger. Second, there are many components represented at the galactic center – young and old disk, thick disk and bar, as well as the inner halo. Interpretation of our results would be more complex there due to the dynamical effect of the bar. The metal-weak tail of the thick disk is also minimized when we look at higher latitudes.

2.2. Tracers

Traditional ways of searching for halo stars include:

- Proper motion surveys (Sandage and Fouts 1987; Carney and Latham 1987; Ryan and Norris 1991). These surveys identify stars at most a few hundred pc away, except for the surveys of Majewski (1992) and Mendez et al. (1999), which produced complete proper motion information on a sample of stars to B=22.5 and 19 respectively (a maximum distance of 30 kpc).

- RR Lyrae surveys (Kinman et al. 1965; Saha 1985; Suntzeff et al. 1991; Wetterer and McGraw 1996; Kinman et al. 1996). These surveys sample more distant objects, but because of their extreme rarity – of order one per deg^2– few distant RR Lyraes are known.

- Objective prism surveys, generally for metal-poor giants or stars near the main sequence turnoff. (Bidelman and MacConnell 1973; Ratnatunga and Freeman 1989; Beers et al. 1985; Morrison et al. 1990). Because of the relatively high resolution needed to identify these stars spectroscopically, these surveys are in general restricted to relatively bright magnitudes and therefore relatively nearby objects.

- Blue horizontal-branch (BHB) star surveys. The BHB stars are identified either from their unusually blue color (Sommer-Larsen and Christensen 1985; Norris & Hawkins 1991) or by using objective prism spectra near the Ca K line (Pier 1982, 1984; Beers et al. 1985). BHB stars are almost as rare as RR Lyrae variables, and their identification is complicated by the presence of halo blue stragglers, which have the same broadband colors as BHB stars but higher gravity. As Norris and Hawkins show, the blue straggler fraction may be as high as 50% for samples of faint blue stars.

- Carbon stars. These are extremely rare stars (of order one per 200 deg^2, Totten and Irwin

1998) which are identified easily from objective-prism spectra. Totten and Irwin (1998) review the currently known halo carbon stars and their properties. Distances are more uncertain for these stars than for any other tracer we have discussed.

Halo tracers we chose to use are:

- Red giants. These are identified photometrically using a luminosity indicator based on the Mg b/MgH feature at 5170Å plus a metallicity indicator based on line blanketing near 4000Å , with spectroscopic confirmation.
- Blue horizontal branch (BHB) stars, identified by their color plus a spectroscopic check of gravity.
- Stars at the main sequence turnoff, identifiable from their blue color — the most metal-poor globular clusters have turnoff colors of $B-V \simeq 0.38$, while the thick disk turnoff is $B-V \simeq 0.5$, so stars with colors between these two values are most likely halo turnoff stars.
- Blue metal-poor stars (Preston et al. 1994), which are halo field stars with colors bluer than $B-V=0.38$, thought to be younger main sequence stars. When found in globular clusters, such stars are typically referred to as blue stragglers and may have a different origin from the field analogs.

We will discuss these tracers, and possible contaminants in our sample, below. We reject another halo tracer, RR Lyrae variables, because of the large amount of telescope time needed to identify and phase these variable stars.

Our technique reliably identifies both turnoff stars from the halo and the more distant halo giants and BHB stars. Because of their different luminosities, these objects probe different regions of the galactic halo. Turnoff stars can only reach to galactocentric distances of 15–20 kpc using 4m-class telescopes for spectroscopic followup, while red giants and BHB stars will reach to distances of more than 100 kpc. However, due both to shorter evolutionary timescales for giants and to the strong decrease in halo density with galactocentric distance ($\rho \propto r^{-3}$ or $r^{-3.5}$, Zinn 1985, Saha 1985), there are far fewer halo giants detected than turnoff stars. Different techniques are therefore used to search for the kinematic signatures of accretion. For the more numerous turnoff stars, we use statistical techniques based on the appearance of the velocity histogram (testing for multimodality, for example, see Harding et al. (1999)). For the rarer red giants, we use the technique of Lynden-Bell and Lynden-Bell (1995) (see also Lynden-Bell 1999) to search for stars with similar energies and angular momenta, indicating a common origin.

3. SELECTION TECHNIQUE

Our initial survey was done using the Burrell and Curtis Schmidt telescopes, which have CCD fields of order 1 deg^2. The Burrell Schmidt is fitted with a back-illuminated SITe 2048×4096 CCD with 1.5 arcsec per pixel, while the Curtis Schmidt (often) has a 2048×2048 back-illuminated Tek CCD with 2.4 arcsec per pixel. Now that large mosaics are available, we have extended the survey using the CTIO 4m with the BTC (field = 0.25 deg^2) and the 8-CCD NOAO mosaics. Our spectroscopic followup observations have been made using the Hydra multiobject fiber spectrograph on the 3.5m WIYN telescope and the RC spectrograph on the KPNO 4m. Future observations with the Hydra spectrograph on the CTIO 4m and the Magellan telescope are planned.

The Washington photometric system combines strong metallicity sensitivity for late-type giants with broad filter passbands, which contribute to observing efficiency. We use this system for our survey, as its filters can be used for selection of all the other tracers we need as well. We describe transformations between the Washington system and the BVI system in the Appendix.

In each survey field (of area approx 1 deg^2) we obtain photometry using a modified Washington (Canterna 1976; Geisler 1984) filter set (C,M, 51 and i' filters). The large pixel area on the Schmidt telescopes leads to a high sky level in the I band. Thus we use the Sloan i' filter, whose passband avoids the worst of the bright sky lines in the I band, in place of the Washington T_2 or I filters. This i' filter transforms readily to the Washington system.

Typical exposure times using back-illuminated CCDs and the 24-inch Schmidt telescopes are 6000 sec in C and M, 8400 sec in 51, and 4800 sec in i'. On the CTIO 4m with the BTC mosaic, exposure times were 100 sec in M, 500 sec in C, 120 sec in T_2 and 250 in 51. These give typical errors of 0.015 mag. in each filter for a V=19 star. Our photometry will be discussed in more detail by Dohm-Palmer et al. (1999).

We have used the data of Schlegel et al. (1998) to estimate the values of reddening in our fields, and de-reddened the Washington colors according to the prescriptions of Canterna (1976) and Harris and Canterna (1979). The reddening values are small, so this did not have a strong effect on our results in any case.

Figure 2 shows a typical color-magnitude diagram with the position of the halo and thick disk turnoffs marked. Since each tracer requires a different selection technique, we will discuss them separately.

3.1. Halo giants

This tracer is the most exciting since it allows us to probe the extreme outer halo. These stars have been little used in the past because they are greatly outnumbered by foreground K dwarfs, and it is difficult to distinguish K dwarfs from giants without accurate intermediate-band photometry

or spectroscopy. However, their potential is enormous: a metal-poor star near the giant branch tip with M_V=–2 and V=19.5 (easily observable at medium resolution on a 4m-class telescope) has a distance of 200 kpc! The combination of large CCD fields with the Washington photometric system makes the detection of such objects feasible for the first time.

These distant halo giants are rare. Using the simple model of Morrison (1993), we find that there are of order 1–10 halo giants per square degree down to V=20, using a range of assumptions about the halo density distribution. In section 4 we will show that out to galactocentric distances of 20 kpc, the halo density law is well described by a flattened power-law with exponent –3.0 and flattening b/a=0.6. If this density law continues to larger distances, we would expect to see 4 halo giants deg^{-2} brighter than V=20 at the NGP and 5 deg^{-2} in an anticenter field with galactic latitude 45°.

There are three classes of objects found in the same range of color and magnitude as the halo giants we wish to find:

- numerous K dwarfs of the thin and thick disk, which can be detected using a photometric survey ($M-51$ color)
- extremely metal-poor halo dwarfs, which are present in comparable numbers to halo giants for $V > 18$, and need a good follow-up spectrum (with S/N$\sim$15) to distinguish from halo giants.
- background objects such as compact galaxies and QSOs, which are easily weeded out using a low S/N followup spectrum.

3.1.1. Disk Dwarfs

The major source of contamination of a halo giant sample is foreground K dwarfs. To quantify the numbers of foreground dwarfs that we will need to weed out, we have estimated their number using a modified version of the Bahcall-Soniera model which includes both thin disk and thick disk, using a 5% normalization for the thick disk. This predicts 70 thin disk dwarfs and 90 thick disk dwarfs ($0.9 < B-V < 1.2$) per deg^2 at the NGP.

Classical spectroscopic luminosity indicators (originally developed for Pop. I stars, eg Seitter 1970) which are useful for our survey include:

- the Mg b triplet and MgH band near 5200Å. These features are much stronger in dwarfs than giants in this color range. They begin to lose sensitivity to luminosity blueward of $B-V = 0.9$ ($M-T_2$=1.2). These features are also temperature sensitive.
- the Ca I resonance line at 4227Å shows marked sensitivity to both luminosity and temperature in K stars. Its strength increases as temperature and luminosity decrease. Since we have an

independent photometric measure of temperature from $M-T_2$ color, we can use the Ca I 4227Å line as a luminosity indicator.

- The blue and UV CN bands (bandheads at 4216 and 3883Å) are strong in giants and not in dwarfs. The bands become weaker with decreasing metallicity, and are not visible below [Fe/H] = –1.5.

We have observed metal-poor dwarfs and giants in order to check whether these indicators retain their usefulness for more metal-poor stars. Our observations, plus those of the metal-weak giants we found, will be discussed in more detail by Olszewski et al. (1999). We use the Mg b/MgH region as our major method of rejecting disk dwarfs in our sample via photometric selection.

Geisler (1984) augmented the original Washington system with the DDO "51" filter, an intermediate-band filter centered on the Mg b and MgH features near 5200 Å , to give luminosity sensitivity for late G and K giants. The $M-51$ color gives a photometric method of measuring the strength of these features. Figures 3(a)–(d) show the strength of the MgH feature in spectra of dwarfs of solar and lower metallicity, and of the Mg b feature for giants of different metallicity. Most of these stars do not have direct measures of $M-T_2$ color. We transformed to Washington colors from existing b–y or $B-V$ colors, using the method discussed in the Appendix. For ease of display we have sorted the stars into bins of metallicity and color. Table 2 gives sources of metallicity and color for all the stars shown in Fig. 3.

These spectra clearly illustrate the luminosity indicators discussed above. A strong MgH band is seen for dwarfs with $M-T_2 = 1.2$. The feature becomes weaker as temperature increases, until it is hard to see in the dwarfs with $M-T_2 = 1.0$. Although we do not have any spectra for dwarfs redder than $M-T_2 = 1.3$, the MgH band continues to strengthen with decreasing temperature. For all except the reddest giants ($M-T_2 > 1.45$) there is no MgH feature visible, and the Mg b lines are weak. For $M-T_2$of 1.45 and redder, there is a slight MgH feature visible for the giants with [Fe/H] = –1.0 and above.

Our main method of detecting foreground dwarfs photometrically is via these features (MgH + Mg b). Other spectral features which are useful for luminosity discrimination with a follow-up spectrum are the Ca I 4227Å line and the CN bands. The Ca I 4227Å line is visible in all the dwarf spectra, and can be seen to increase in strength as temperature decreases. It is also visible in the spectra of the metal-poor giants (especially above [Fe/H] = –1.5) but is much weaker than in dwarfs of the same color. Blue and UV CN bands are visible in the metal-richer giants (for example M71 stars l-1, S232) and will be discussed in more detail in the next section.

The 51 filter gives us the ability to measure the strength of the MgH feature and reject the numerous foreground dwarfs. Precise photometry is necessary, however: Geisler (1984) obtained $M-51$ colors for a sample of metal-rich and metal-poor giants, and predominantly metal-rich dwarfs. He showed that giants and metal-rich dwarfs differ by at least 0.10 mag in M-51 color for $B-V > 0.85$, and that the difference becomes more pronounced between metal-poor giants (with

weaker Mg b) and metal-rich dwarfs.

Figure 4 shows $M-51$colors for known dwarf and giant stars. Geisler (1984) plotted $M-51$ versus $T_1 - T_2$; it is clear from Fig. 4 that the use of $M-T_2$ as a color does not degrade the luminosity sensitivity. Our measurement errors for $M-51$ are 0.02 to 0.04 mag., allowing us to discriminate easily between giants and all dwarfs except the most metal-poor using our photometric survey.

Because we are searching for intrinsically very rare objects, we are particularly vulnerable to photometric errors — dwarfs with 3-sigma errors in their colors are more common than our most distant halo giants. Since all but a few percent of the known halo stars have [Fe/H]<–1.0, we can use metallicity as an additional criterion. We use an additional Washington filter to identify halo giants: C. $C-M$ is a metallicity indicator which was calibrated for giants by Geisler et al. (1991). We require that candidates lie in the [Fe/H] < -1.0 region of the Washington $C-M$ vs. $M-T_2$ diagram.

Figures 5 and 6 show how successful our photometric classification has been. Photometric data from 22 high-latitude fields observed at the CTIO 4m with the BTC in April 1999 are plotted with spectroscopic confirmations shown as larger symbols. These data will be described in more detail by Dohm-Palmer et al. (1999). Note that we deliberately chose to observe candidates near the giant/dwarf boundary to mark it carefully for future work.

3.1.2. Extreme K subdwarfs

Metal-poor halo dwarfs are of particular concern because their spectra more closely resemble metal-poor giants. The Bahcall-Soniera model (Bahcall and Soniera 1984) predicts that 15 halo dwarfs will be found per square degree down to V=20 in the color range that we search for giants ($B-V=$ 0.9 to 1.2). (Recall from Section 3.1 that we expect to see 4-5 halo giants in the same magnitude interval.)

There are very few metal-poor K dwarfs with $M-51$ photometry available, so we cannot accurately measure the photometric separation between metal-poor dwarfs and giants. However, Paltoglou and Bell (1994) have calculated synthetic $M-51$ colors for their grid of dwarf and giant models of different metallicity. These models are based on the linelists of Bell et al. (1994). We show their dwarf sequences for [Fe/H] from 0.0 to –3.0 in Fig. 4. It can be seen that the most metal-poor dwarfs, with [Fe/H] $<$ –2.0, overlap the region where giants are found in this diagram. Thus, the models suggest that the $M-51$ photometric index will not be useful for weeding out the extreme K subdwarfs in our fields — we will need to examine their spectra in more detail.

How common are these extremely metal-poor subdwarfs? We can estimate the number of halo dwarfs with [Fe/H] $<$ –2.0 using the halo metallicity distribution of Ryan and Norris (1991); 31% of their sample has [Fe/H] $<$ –2.0, which, in conjunction with the results of the Bahcall/Soniera

model, translates to 4 very metal-poor halo dwarfs per deg^2 for $V < 20$ at the NGP. Halo dwarfs only appear in significant numbers for $V > 18$, but the very distant halo giants also have $V > 18$. We need to consider these contaminants seriously.

We have approached the problem of discriminating spectroscopically between halo giants and extreme K subdwarfs in two ways — by obtaining spectra of the few extremely metal-poor K dwarfs known in this temperature range, and supplementing these with synthetic spectra. It is practical to depend on follow-up spectroscopy to weed these objects out because of their rarity.

Since some of the major differences between K dwarfs and giants are due to molecular bands, we have used the NextGen model atmosphere grid (Hauschildt et al. 1999a,b) for the synthetic spectra. These models were originally designed to model the atmospheres of very low-mass stars and brown dwarfs, and include a detailed molecular equation of state and a set of molecular opacity sources which improve on those used in previous work. Hauschildt et al. (1999a) state that their models are more suitable for stars with $T_{eff} < 5000$K than previous models such as that of Kurucz (1992).

The NextGen models are described in Hauschildt et al. (1999a,b). Peter Hauschildt kindly computed NextGen models with [Fe/H] = –2.0 and an over-abundance of the alpha elements similar to that seen in halo stars ([α/Fe]=0.4) for us. They were calculated with log g = 1.0 and 4.5 to match giants and dwarfs with effective temperatures of 4700 and 4500K. The model spectra are shown in Fig. 7, smoothed to the same resolution as our 4m spectra. It can be seen that there are marked differences between giants and dwarfs with [Fe/H]=–2. Both dwarf models, especially the cooler one, show MgH features, and both show strong lines of Ca I 4227, unlike the giants, and much stronger Mg *b* lines. The dwarfs also show much stronger lines in the region blueward of the Ca H and K lines, particularly in the region near 3840 Å where lines of FeI and MgI contribute.

In the next two figures we focus on two regions of the spectrum which are particularly useful for luminosity discrimination, comparing spectra of known metal-poor dwarfs and giants and supplementing with synthetic spectra when no real spectra are available.

Fig 8 shows the region between 3700 and 4500Å . It can be seen that the most metal-poor dwarf for which we have a spectrum, HD 134440 with [Fe/H]=–1.5 and T$_{eff}$=4740K (Carbon et al. 1987) matches the model spectrum with [Fe/H]=–2.0 and T$_{eff}$=4700K quite well, giving confidence in the synthetic spectra. There is no marked difference in G band strength between giants and dwarfs, but all the dwarf spectra show a strong feature at Ca I 4227. The metal-poor giants of moderate metal deficiency ([Fe/H] $\geq$ –1.6) show a weaker Ca I line, while the very metal-poor giant shows almost none.

The blue and UV CN bands are also visible in the giants with [Fe/H] $\geq$ –1.6, while the dwarf spectra look quite different in this region. The feature just blueward of 3840Å is very strong in the dwarfs, and is significantly narrower than the UV CN band. We note that because of CN anomalies in globular clusters, the CN strength of the stars in Fig 8 may not be typical of field stars. While CN measurements of the three globular cluster giants shown in the Figure are not available, field

giant stars do show these CN features, as can be seen in Figure 4(b) of Flynn and Morrison (1990). This criterion can be used as a way of confirming that a star is a giant, because no dwarf shows these CN features. It cannot be used as a way of confirming that a star is a dwarf because some giants may be CN weak.

Fig. 9 shows the region from 5000 to 5300Å . While the large-scale shape of the MgH band is not easily visible when such a small region of spectrum is displayed, it can be seen that at a given $M-T_2$color, both the MgH bandhead and the Mg triplet are stronger in the subdwarfs than in any of the giants. Even the M71 giants, whose metallicity is higher than we aim to identify in our halo sample, are distinguishable from subdwarfs. However, the effect is too small to depend on the $M-51$ color to identify these subdwarfs reliably.

In conclusion, our photometric survey will weed out the more common dwarfs of the thin and thick disk, but is unable to identify the very metal-poor K subdwarfs of the halo. These stars are rare enough that it is practicable to use follow-up spectra with good S/N to reject them. We can measure our success rate for photometric pre-selection using the percentages of spectroscopically confirmed giants, foreground dwarfs and subdwarfs. 70% of giant candidates in the correct region of the $M-51$ vs.$M-T_2$ diagram were giants, 20% were subdwarfs and 10% were dwarfs. Given our expected lack of success in discriminating subdwarfs from giants photometrically, this confirms that our photometric selection technique is very effective.

Figure 10 illustrates the success of our selection with spectra of metal-poor giants identified in our survey. Metallicity and distance values obtained from the Washington $C-M$ vs. $M-T_2$ calibration are given for each star. Our sample already includes two stars which are more distant than the LMC, one of which is shown in Fig. 10, and we are well placed to discover a large number of giants in the outer halo where only dwarf satellites and globular clusters were previously known.

3.1.3. Extragalactic Contaminants

Possible extragalactic contaminants of our giant sample are QSOs and unresolved galaxies. Reid & Majewski (1993) show that there are ~ 15 QSOs and unresolved galaxies deg^{-2} down to R=19 at the NGP.

Most QSOs are separable photometrically because of their unusual positions in the color-color diagram, although a few need to be weeded out spectroscopically. However, color discrimination does not work for unresolved normal galaxies, as their integrated colors are similar to those of metal-poor giants (Geisler 1995). The large pixels on the Schmidt telescopes mean that we are more vulnerable to this problem there. With smaller pixels the galaxy contamination is much less severe — on our recent 4m run (reported in Olszewski et al. (1999)) where fourteen halo giants were identified from CTIO 4m/BTC data, no galaxies were mistakenly found.

3.2. Blue Horizontal-Branch Stars

These stars will cover a distance range of 5 – 50 kpc, and thus represent another important tracer of the outer halo in our survey. The number of BHB stars per deg^2 depends on the horizontal-branch morphology of the halo field, which is not well determined for large distances from the Galaxy's center. If the halo field follows the globular clusters in having a redder horizontal branch morphology for large radii, then we would expect a few BHB stars per deg^2 in the magnitude range V=15–20.

We restrict ourselves to the portion of the horizontal branch which is flat in V magnitude, between $B-V$=0.0 and 0.20. This converts to a color range of 0.0 to 0.30 in $M-T_2$ (see Fig. 20).

It can be seen from Figure 2 that this is a sparsely-populated portion of the color-magnitude diagram, and the only non-halo contaminants of our sample in this color range are white dwarfs and QSOs. There are 3 white dwarfs deg^{-2} and 5 QSOs deg^{-2} down to V=20 in this color range, Fleming et al. (1986); Sandage and Luyten (1969); Reid & Majewski (1993). Both of these types of objects are easy to discriminate with even a low-dispersion, low signal-to-noise spectrum.

We also need to be able to discriminate between halo blue stragglers (with main sequence gravities) and blue horizontal branch stars. Our followup spectroscopy allows us this via Balmer line profiles (Pier 1983; Sommer-Larsen and Christensen 1985; Norris & Hawkins 1991; Kinman et al. 1994). In cases where we are able to obtain spectra which reach below the Balmer jump, its size can also be used as a discriminator. Kinman et al. (1994) used spectra of 3.7Å resolution (very similar to our 4m spectral resolution) to make this measurement.

Figure 11 shows spectra of known BHB standards and two BHB stars from our sample.

3.3. Halo turnoff stars

Halo turnoff stars are the most numerous but least luminous tracers we shall use, and sample distances from 2 – 16 kpc from the Sun (assuming an absolute magnitude $M_V = 4.5$ and a limiting magnitude of V=20.5).

We used the halo turnoff luminosity function calculated in Section 4.1 and the preferred halo model from Section 4 (power law exponent of –3.0 and an axial ratio of 0.6) to calculate the numbers of turnoff stars per square degree we would expect to see in our fields. Under these assumptions, there should be 150 halo turnoff stars per square degree down to V=20.5 at the NGP, and 130 per square degree in the anticenter at b=45.

These stars are relatively easy to identify using accurate photometry because they are bluer than almost all stars at high galactic latitude. For the most metal-poor globular clusters such as M92, the turnoff is at $B-V$=0.38, significantly bluer than the turnoff color of the thick disk ($B-V$=0.5, Carney et al. (1989)). The thin disk has a sufficiently small scale height that very

few young thin disk stars are found in our magnitude range at high galactic latitude (Bahcall and Soniera 1984). We choose stars with $B-V$ color of 0.38 to 0.49 as halo turnoff star candidates.

The transformation to $M-T_2$ color is complicated by the fact that we have no observations of metal-poor turnoff stars in this color. We approach the problem in two ways. First, only the most metal-poor stars will have a turnoff color as blue as $B-V = 0.38$, so we could use the synthetic colors of Paltoglou and Bell (1994) for their models with [Fe/H] = –2.0 to derive the transformation. This predicts a turnoff color of $M-T_2$=0.6. Second, we can derive the turnoff color using $V-I$ and Stromgren photometry of metal-poor globular clusters from the literature. Table 3 summarizes the turnoff colors in $V-I$ and $b-y$ of metal-poor globular clusters NGC 6397, NGC 7099 and M92, and the metal-rich cluster 47 Tucanae. The average $V-I$ turnoff color for these three metal-poor clusters is 0.51, which transforms via Fig. 19 to $M-T_2$=0.64. Thus the estimates from theory and observation are in reasonable agreement, and we have chosen to use the observational estimate here. We also use the $V-I$ photometry of Kaluzny et al. (1998) for 47 Tuc to constrain the turnoff color of the thick disk to be $M-T_2$=0.81. In summary, we take the color range from $M-T_2 = 0.64$ to 0.80 for our halo turnoff stars. As a consistency check on our photometry, we also require that $C-M$ is in the range 0.2 to 0.5.

Thick disk stars scattering into the color range should be a minor problem because of our small photometric errors (our $M-T_2$ errors are less than 0.02 mag. at V=19) and the fact that we work faint enough to be away from the regions of the Galaxy where the thick disk dominates. Using the models of turnoff stars in the thick disk and halo of section 3.1, we can show that only for the brightest part of our magnitude range (V=16–17, corresponding to distances of order 2.5 kpc, saturated on 4m/BTC data but not on Schmidt data) are numbers of thick disk stars per square degree greater than halo star numbers in our fields, and then only by a factor of $\sim$2, which is not large enough to make significant numbers of thick disk stars "leak" into the halo color range via photometric errors. For stars with V=17–18, numbers of thick disk and halo turnoff stars are approximately equal, and for fainter magnitudes, halo turnoff stars outnumber thick disk stars.

The only other contaminants of our sample in this color range are small numbers of white dwarfs, QSOs and RR Lyraes. The QSOs and white dwarfs are obvious from spectra, and the RR Lyraes are sufficiently rare that few will be detected and some of these will be removed due to their variability on either photometric or spectroscopic observations.

Figures 2 and 14 illustrate the selection technique, showing color-magnitude diagrams ($M-T_2$ vs M) for a single field and for a composite of many fields. The position of the turnoff for both halo and thick disk is marked, and our candidate halo turnoff stars are shown. With very few exceptions, all stars in this region of the CMD show spectra typical of halo stars, i.e. metal-poor. Figure 12 shows WIYN/Hydra spectra of several of these stars. It is clear that the halo turnoff candidates are indeed metal-poor, confirming the accuracy of our photometry.

3.4. Blue Metal-Poor Stars

Preston et al. (1994) identified an important group of halo turnoff stars with color bluer than $B-V = 0.38$, and suggested that these stars were metal-poor stars with unusually young ages, which had originated in dwarf spheroidal satellites which were subsequently accreted into the Galaxy's halo. Another possibility is that these stars are the result of the evolution of multiple star systems of the halo. Preston has obtained detailed follow-up spectroscopy of a number of these stars to test this possibility. Preston et al. (1994) estimated numbers in the solar neighborhood of 350–450 per kpc^3 (cf. the density from Table 4 of 2695 halo turnoff stars per kpc^3 with M_V=4.5). Unavane et al. (1996) found from photographic starcount data that $\sim 10\%$ of halo stars were bluer than $B-V$ = 0.4, which is in rough agreement with the Preston et al. (1994) value. These BMP stars are particularly important for our survey if they have younger ages, and we select them by $B-V$ color between 0.15 and 0.35 ($M-T_2$ = 0.2 to 0.6).

Using the Preston et al. (1994) local normalization, we expect to find 10–20 BMP stars deg^{-2} to V=19. Our Fig 2 shows 23 such stars in the color range $M-T_2$ = 0.2 to 0.6 for an area of 2.75 deg^2, a little lower but not significantly different from the value of Preston et al. (1994).

4. MAPPING THE HALO – "INTELLIGENT" STAR COUNTS

Accurate CCD photometry of large areas in many fields makes an new method of investigation of the halo possible. As discussed in Section 3.3, the halo turnoff color is $B-V$= 0.38, and the thick disk turnoff is $B-V\sim$ 0.5, so stars with colors between these two numbers are almost certainly halo stars close to the turnoff. Photographic colors have such large errors (0.05 to 0.10 magnitudes) that it is not possible to isolate halo turnoff stars from photographic data without simultaneously modelling the contribution of the thick disk. In contrast, our photometry is of such high and uniform quality that it is possible to separate halo turnoff stars cleanly from thick disk turnoff stars using the $M-T_2$color. Fig. 14 illustrates this in one of our lowest latitude fields, where both thick disk and halo turnoffs can be seen.

We now make a preliminary analysis of the BTC data to illustrate the power of our survey technique. Our major aim here is to check whether our data agree with other models for the halo.

The dataset obtained with the Big Throughput Camera on the CTIO 4m in April 1999 (Dohm-Palmer et al. 1999) is particularly useful for mapping the halo because of the uniform quality of the data, and the fact that conditions were photometric throughout the run. Fig. 13 shows in cartoon form the location of the fields where data were obtained. There are 46 fields with latitudes ranging from +25 to +73, and longitudes from l=17 through the galactic center to l=218 (less than 40 degrees from the anticenter).

We have checked for errors in reductions or reddening estimation by carefully examining the color-magnitude diagrams of all fields. Figure 14 is typical: the position of the halo turnoff is clear,

and agrees well with the calculated value of $(M-T2)_0$=0.64 in all but two of the 46 fields. In these two fields it appears that the Schlegel reddening values that we used should be adjusted by a few hundredths in order to bring the turnoff position to this color. Because the stars are uniformly distributed across the color range from $(M-T2)_0$=0.64 to 0.8, photometric errors or reddening estimates of a few hundredths of a magnitude will in no case be strong enough to make the turnoff star numbers vary significantly.

Models of the shape of the halo have in many cases been derived from easily detectable tracers such as globular clusters (Zinn 1985) or horizontal-branch stars (Kinman et al. 1965; Saha 1985; Hartwick 1987; Preston et al. 1991; Kinman et al. 1994). Studies using star counts (eg Bahcall and Soniera 1986) are handicapped by their inability to separate halo and thick disk accurately with photographic photometry, as discussed above. Models from both globular clusters and field stars both find that the halo is centrally concentrated, with power-law exponent varying from –3.0 to –3.5 or even steeper. Axial ratios vary from 0.5 to 1.0, with suggestions from several groups that the axial ratio might change with galactocentric radius in the sense that the outer halo is spherical and the inner halo flattened.

However, neither globular clusters nor horizontal-branch stars are ideal for measuring the density distribution of the halo. First, it is not clear that the halo field stars were formed under the same conditions as the globular clusters. Second, possible age and metallicity gradients in the halo (Searle and Zinn 1978; Zinn 1993; Preston et al. 1991; Kinman et al. 1994) are reflected in horizontal-branch morphology. This can cause a different power-law exponent to be derived for RR Lyraes and BHB stars, as found by Preston et al. (1991). Thus a check of the earlier results with a different tracer is valuable. Although our turnoff star sample will also be sensitive to age and metallicity variations, we are able to check for such effects by examining the color-magnitude diagrams of discrepant fields directly.

4.1. Local Halo Density

The estimation of the halo density in the solar neighborhood is even more challenging than the measurement of its density in more distant fields. It has in most cases been based on the local density of stars selected by their high proper motion (eg Bahcall and Casertano 1986), with kinematic corrections made for the amount of the halo that would be missed using this selection technique. There have also been a small number of direct measurements of local density of some tracer such as RR Lyraes or red giants (eg Preston et al. 1991, Morrison 1993) which agree within a factor of two with the proper-motion data, but different selection effects such as metallicity operate for these samples. Attempts to extrapolate the results of pencil-beam surveys inward to the solar neighborhood are not always successful — Preston et al. (1991) and Wetterer and McGraw (1996) note the disagreement of a factor of two between the counts of nearby RR Lyrae variables and the extrapolation of more distant RR Lyrae counts inward.

Since we have few low-latitude fields and our BTC data saturate for magnitudes much brighter than V=17 (corresponding to a distance of 3 kpc for turnoff stars) we have no direct constraints on the local density from our data. Our preferred value of the solar neighborhood halo density will depend on the axial ratio adopted.

We decided to re-examine the measurement of the local halo density from the proper-motion samples, as there have been significant advances in the information available on these stars since the work of Bahcall and Casertano (1986). We have used the extended sample of Carney et al. (1994), which has been updated recently to have a distance scale consistent with the Hipparcos parallax measurements for subdwarfs, to make an estimate of the local density. Bruce Carney kindly made this sample available to us in advance of publication. Also, in order to make comparisons with our BTC data easier, we isolated stars in the turnoff star color bin we used ($B-V$ between 0.38 and 0.5, corresponding to $M-T_2$ between 0.64 and 0.8), and then derived a local luminosity function for these stars alone. Since this is a kinematically selected sample, we need to make corrections for the halo stars missed because of the proper motion selection. To minimise contamination of the sample by thick disk stars, which contribute strongly to the derived local density because the lowest velocity stars are given the highest weights (see Bahcall and Casertano 1986) we only used stars with tangential velocity greater than 220 km/s, and rejected all stars with [Fe/H] > –1.0. This may reject a few genuine halo stars, but will cause an error of only ∼10% in the derived density (Carney et al. 1989). Erroneously including thick disk stars would have a much larger effect.

The Carney et al. (1994) sample is drawn from the Lowell Proper Motion Catalog which covers the entire Northern Hemisphere and has a proper motion lower limit of 0.26 $''$ yr^{-1}. In the color range of concern here, the catalog's magnitude limit is sufficiently faint that all we need to do is correct for proper motion selection effects, which we do by weighting by V_{tan}^{-3}, following Bahcall and Casertano (1986). Table 4 gives our results. Carney and collaborators have a more complete kinematical analysis in progress, so we have chosen simply to use the simulations of Bahcall and Casertano (1986) to correct for the tangential velocity cut at 220 km/s. Morrison (1993) notes that the sample used by Bahcall and Casertano to derive halo kinematics was probably contaminated by thick disk stars, and calculates that the "discovery fraction" for a sample with this V_{tan} cutoff should be close to 0.5, not 0.33 as they found. We have used this higher value in our calculations of the turnoff star luminosity function.

4.2. Halo concentration and axial ratio

While our maps of the halo based on accurate color-magnitude diagrams are less sensitive to possible variations in age and metallicity than the estimates from horizontal-branch stars in particular, they are less easy to interpret because of the difficulty of obtaining accurate distances to turnoff stars. Turnoff stars in our chosen color range can have absolute magnitudes which vary from 3.5 to 5.5, although the luminosity function of Table 4 shows that many will have absolute magnitude near 4.5. We have chosen to divide our data into three magnitude ranges (V=17–18.5,

18.5–19.5 and 19.5–20.5) and to calculate model predictions for these magnitude ranges to compare directly with the star counts there. We plan to do a more statistically sophisticated analysis in a future paper — the values we derive here will be roughly correct for the distance ranges probed by the data, but not may not be optimal.

Fig. 15 shows the sensitivity of our data to the axial ratio of the halo. It shows the ratio of number of stars in a given magnitude bin to the model predictions. Both models have a power-law exponent of –3.0, and one has an axial ratio b/a=1.0 (spherical) while the other has a moderate flattening (b/a=0.6). We have plotted these ratios vs a rough indicator of the z height travelled by each line of sight, calculated by assuming that all stars in the bin have absolute magnitude M_V=4.5. It can be seen in Fig. 15 that the spherical halo provides a significantly worse fit. There is a trend with z: points with high z have fewer stars than the model predicts, and points with low z have more. The b/a=0.6 model residuals show little trend with z, and the small number of very discrepant points remaining are found with both small and large z.

Fig. 16 shows the same data/model ratios against the range in R_{gc}, for models with b/a=0.6 and power-law exponent –3.0 and –3.5. A trend with R_{gc} is visible in the panel with power-law exponent of –3.5. The model predicts too few stars with large R_{gc} and too many with small R_{gc}. Note also that in the panel showing residuals from the model with exponent –3.0, the remaining residuals show no clear trend with R_{gc}. We adopt a model with b/a=0.6 and power-law exponent –3.0 for the rest of this analysis. Only a 10% correction to the local halo density of Table 4 is needed with these parameters.

It is possible to examine the residuals to the model fits in more detail by plotting the position in the Galaxy traversed by each field, and highlightling the fields with large residuals. Figures 18 and 17 show a number of vertical and horizontal slices through the Galaxy, for different ranges of y and z. Fields with residuals more than 2.5σ from the model fit are highlighted. It can be seen that four of the fields with large negative residuals are towards the galactic center, and two, with large positive residuals, are in our lowest latitude field, which is close to the anticenter. Interestingly, the discrepant fields cover a large range in both r and z, so a simple adjustment to the power-law exponent or flattening will not improve things.

The variable axial ratio models of Hartwick (1987) and Preston et al. (1991) will not solve the problem completely. The model of Preston et al. (1991) has an axial ratio changing linearly from b/a=0.5 at the galactic center to b/a=1.0 for ellipsoids with semi-major axis of 20 kpc. While the results in fields close to the minor axis which currently have large negative residuals may be improved by the adoption of a model where the axial ratio is closer to 1 at this point, the anticenter fields will become more discrepant since the axial ratio must become close to 1 at this distance from the center too. However, it is possible that the thick disk might be partially responsible for the excess of stars in this color range, if its scale height increases in the outer Galaxy and/or it has a strong abundance gradient.

We plan to investigate these issues further when we obtain more fields with low values of R_{gc}

and z.

5. CONCLUSIONS

We describe a survey designed to find field stars from the galactic halo in large enough numbers to provide a strong test of the question "Was the galactic halo accreted from satellite galaxies?"

The survey will cover 100 deg^2 at high galactic latitude. It uses an efficient pre-selection technique based on the Washington photometric system to identify halo red giants, blue horizontal branch stars, blue metal-poor main sequence stars and turnoff stars. Follow-up spectroscopy (with multi-object spectrographs for the more numerous turnoff and BMP stars) tests for kinematic signatures of accretion. Our sample of halo stars will be unprecedentedly large, and cover galactocentric distances from the solar circle to more than 100 kpc. Because the photometric selection has few and easily quantifiable selection effects, our sample will also enable thorough studies of the density distribution of the galactic halo, increasing the numbers of distant halo objects known by an order of magnitude. This will allow much more accurate measurement of the mass of the Galaxy than previously possible.

We discuss the particular problems caused for identification of the very distant halo giants by foreground K subdwarfs with very low metallicity ([Fe/H]<–2.0). These stars are roughly as numerous as the genuine halo giants for $V > 18$, and are not distinguishable from giants via the Washington $M-51$filter that we use for photometric luminosity discrimination. However, with low-dispersion spectra of S/N 15 or more, a combination of several spectral features such as the Ca I line at 4227 Å suffices to distinguish these stars reliably from giants. Studies which use giants in the outer halo need to take particular care to eliminate these extreme K subdwarfs.

We use one of our large photometric datasets, obtained in one run using the BTC on the CTIO 4m, to constrain the spatial distribution of the Galaxy's halo over ranges of galactocentric distances from approximately 5–20 kpc and z heights from 2 to 15 kpc by using halo turnoff star numbers. We find that a power-law with exponent –3.0 and a moderate flattening of b/a=0.6 gives a good fit to most of the data. However, there are a number of fields that show departures from this model, suggesting that we will need a more complex model in future as our coverage of fields in the halo increases.

It is a pleasure to thank Peter Hauschildt for kindly running the alpha element-enriched NextGen models for us and making the NextGen models so readily available on the Web. We would also like to thank Doug Geisler for the careful work he has devoted to making the Washington system so useful, and for his help with our many questions about the system, and Bruce Carney for kindly making his database available in advance of publication. We have benefited from

helpful discussions with Mike Bessell, Bruce Carney, Conard Dahn and Peter Dawson. We would also like to thank an anonymous referee for comments that improved this paper.

This work was supported by NSF grants AST 96-19490 to HLM, AST 95-28367, AST96-19632 and AST98-20608 to MM, and AST 96-19524 to EWO. We used the SIMBAD database, maintained by CDS, Strasbourg, extensively.

APPENDIX: CONVERSIONS BETWEEN WASHINGTON AND OTHER SYSTEMS

The Washington broadband photometric system (Canterna 1976; Harris and Canterna 1979; Geisler 1996) includes the T_2 filter (which is very similar to the Cousins I filter), the M filter (which is 1050Å wide and has a central wavelength of 5100Å, slightly blueward of the V filter) and the C filter (which is 1100 Å wide, centered near the Ca K line at 3934 Å). Geisler (1984) has added the DDO "51" filter to make giant/dwarf discrimination possible for G and K stars. (The system also includes the T1 filter, similar to the Cousins R filter, which we do not need to use).

The original temperature indicator for the Washington system was the $T_1 - T_2$ $(R - I)$ color. However, an alternative is the $M-T_2$ color, which transforms well to $V-I$ as can be seen in Figure 19. For $V-I$ between 0.5 and 1.5, the simple linear relation $M-T_2 = 1.264$ $(V-I)$ works well. The standard deviation of the residuals from this line is 0.25 magnitudes.

We have included both dwarfs and giants in this diagram, and a significant number of metal-poor globular cluster giants. We used:

- Landoldt (1992) standard stars which are also Washington standards (Harris and Canterna 1979; Geisler 1984, 1986, 1990; Geisler et al. 1991, 1992; Geisler 1996). Only stars with E$(B-V)$ less than 0.11 mag, from the reddening maps of Schlegel et al. (1998) are shown. We corrected the colors using the relations between E$(B-V)$ and the extinction in the Washington passbands using the ratios from Harris and Canterna (1979).

- we used photometry of stars from three globular clusters: 47 Tucanae, NGC 1851 and NGC 6752. The $V-I$ photometry is from Da Costa and Armandroff (1990), and the Washington photometry from Geisler (1986); Geisler et al. (1997).

- Accurate photometry of a sample of very nearby dwarfs was obtained by Gonzalez and Piché (1992). They also measured $B-V$ colors for these stars. Although the authors did not measure $V-I$ colors, Bessell (1979) has shown that the Stromgren $b-y$ color transforms very well to $V-I$ and we have used his transformation, and the very accurate $b-y$ measurements of Eggen (1998), to derive $V-I$ colors for these stars. We have used the six stars in their sample with $B - V \leq 0.51$ to supplement the Landolt standards. Because these stars are so nearby (all have large and accurate parallaxes) reddening corrections are not needed.

It is clear that there is no metallicity dependence in the transformation from $M-T_2$ to $V-I$.

It is also possible to transform the M–T_2 color to $B-V$ but this is less straightforward because there are different loci for late-type dwarfs and giants in this diagram. However, for bluer stars such as halo turnoff stars, the relation is single-valued, as can be seen in Figure 20. Since there are few metal-poor dwarfs with Washington photometry, we have also plotted the models of Paltoglou and Bell (1994) which are based on synthetic spectra, for dwarfs with solar abundance and [Fe/H] = –2.0. Paltoglou and Bell (1994) note that their models show good agreement with existing data for temperatures higher than 4500 K ($B-V \simeq 1.0$).

Washington $C-M$ is less useful as a temperature indicator because it has both metallicity sensitivity for late-type stars (from line blanketing around 4000 Å) and some gravity sensitivity for earlier types (from the Balmer jump) We give the relation between $C-M$ and $B-V$ in Figure 21 for completeness.

It is also useful to derive transformations between the Stromgren $b-y$ color and $M-T_2$. This is particularly useful for K star temperatures, because many of our spectroscopic luminosity standards have b–y observations but not M–T_2. For main sequence stars, we used the compilations of Eggen (1998); Gonzalez and Piché (1992) of photometry of stars from the Yale Parallax Catalog (van Altena et al. 1991), whose stars have the advantage that they are so close to the Sun that reddening corrections are unlikely to be needed. For metal-poor giants we used stars from Bond (1980) with Washington photometry in Geisler (1986). E($B-V$) values were taken from Bond (1980), and were smaller than 0.04 in all cases.

Figure 22 shows the relation between these two colors. It can be seen that there are different sequences for red dwarfs and giants, but that the sequences are fairly tight in both cases.

REFERENCES

Anthony-Twarog, B.J., Twarog, B.A. & Suntzeff, N.B. 1992, AJ, 103, 1264

Armandroff, T.E. & Da Costa, G.S. 1991, AJ, 101, 1329

Bahcall, J.N. & Soniera, R.M. 1984, ApJS, 55, 67

Bahcall, J.N. & Casertano, S. 1986, ApJ, 308, 347

Barbuy, B., Erdelyi-Mendes, M. & Milone, A. 1992, A&AS 93, 235

Beers, T.C., Preston, G.W. & Shectman, S.A. 1985, AJ, 90, 2089

Bell, R.A., Paltoglou, G. & Trippico, M.A. 1994, MNRAS, 268, 771

Bessell, M.S. 1979, PASP, 91, 589

Bessell, M.S. 1990, A&AS 83, 357

Bidelman, W.P. & MacConnell, D.J. 1973, AJ, 78, 687

Bond, H.E. 1980, ApJS, 44, 517

Canterna, R.W. 1976, AJ, 81, 228

Carbon, D.F., Barbuy, B., Kraft, R.P., Friel, E.D. & Suntzeff, N.B. 1987, PASP, 99, 335

Carney, B.W. 1979, ApJ, 233, 211

Carney, B.W. & Latham, D.W. 1987, AJ, 93, 116

Carney, B.W., Latham, D.W. & Laird, J.B. 1989, AJ, 97, 423

Carney, B.W., Latham, D.W., Laird, J.B. & Aguilar, L.A. 1994, AJ, 107, 2240

Ciardullo, R., Jacoby, G.H. & Bond, H.E. 1989, AJ, 98, 1649

Côté, P., Welch, D.L., Fischer, P., & Irwin, M.J. 1993, ApJ, 406, L59

Croswell, K., Latham, D.W., Carney, B.W., Schuster, W. & Aguilar, L.A. 1991, AJ, 101, 2078

Cudworth, K.M. 1979, AJ, 84, 1312

Cudworth, K.M. 1985, AJ, 90, 65

Da Costa, G.S. & Armandroff, T.E. 1990, AJ, 100, 162

Davis, M.M. et al 1985, ApJ, 292, 371

Dohm-Palmer, R.C., Mateo, M.L., Harding, P., Olszewski, E.W., Morrison, H.L., Freeman, K.C. & Norris, J.E. 1999, in preparation.

Eggen, O. J., Lynden-Bell, D., & Sandage, A. R. 1962, ApJ, 136, 748

Eggen, O.J. 1998, AJ, 115, 2397

Fleming, T.A., Liebert, J. & Green, R.F. 1986, ApJ, 308, 176

Flynn, C. and Morrison, H.L. 1990, AJ, 100, 1181

Flynn, C., Sommer-Larsen, J., Christensen, P.R. & Hawkins, M.R.S. 1995, A&AS 109, 171

Geisler, D. 1984, PASP, 96, 723

Geisler, D. 1986, PASP, 98, 762

Geisler, D. 1990, PASP, 102, 344

Geisler, D. 1995, private communication

Geisler, D. 1996, AJ, 111, 480

Geisler, D., Claria, J.J. & Minniti, D. 1991, AJ, 102, 1836

Geisler, D., Minniti, D. & Claria, J.J. 1992, AJ, 104, 627

Geisler, D., Claria, J. & Minniti, D. 1991, PASP, 109, 799

Gonzalez, G. & Piché, F. 1992, AJ, 103, 2048

Governato, F., Moore, B., Cen, R., Stadel, J., Lake, G. & Quinn, T. 1997, NewA, 2, 91

Gunn, J.E. 1995, AAS 186, 44.05

Harding, P.,Morrison, H.L.,Mateo, M.L., Olszewski, E.W., Freeman, K.C. & Norris, J. 1999, in preparation.

Harris, H.C., and Canterna, R.W. 1979, AJ, 84, 1750

Harris, W.E. & Stetson, P.B. 1988, AJ, 96, 909

Hartwick, F.D.A. 1987, in The Galaxy, edited by G. Gilmore and B. Carswell (Reidel, Dordrecht), p281

Hauschildt, P.H., Allard, F. & Baron, E. 1999, ApJ, 512, 377

Hauschildt, P.H., Allard, F., Ferguson, J., Baron, E. & Alexander, D. 1999, ApJ in press, to appear November 1999

Hawkins, M.R.S. 1984, MNRAS, 206, 433

Helmi, A., White, S.D.M., de Zeeuw, P.T. & Zhao, H-S. 1999, Nature, 402, 53

Hesser, J.F., Harris, W.E., Vandenberg, D.A., Allwright, J.W.B., Shott, P. & Stetson, P.B. 1987, PASP, 99, 739

Ibata, R.A., Gilmore, G. & Irwin, M.J. 1994, Nature, 370, 194

Johnson, J.A. & Bolte, M. 1998, AJ, 115, 693

Johnston, K.V., Hernquist, L. & Bolte, M. 1996, ApJ, 465, 278

Johnston, K.V., Spergel, D.V. & Hernquist, L. 1995, ApJ, 451, 598

Kaluzny, J. Wysoka, A., Stanek, K.Z. & Krzeminski, W. 1998, Acta Astronomica, 48, 439

Kinman, T.D., Wirtanen, C.A., & Janes, K.A. 1965, ApJS, 11, 223

Kinman, T.D., Suntzeff, N.B & Kraft, R.P. 1994, AJ, 108, 1722

Kinman, T.D., Pier, J. R., Suntzeff, N. B., Harmer, D. L., Valdes, F., Hanson, R. B., Klemola, A. R. & Kraft, R. P. 1996, AJ, 111, 1164

Klypin, A., Kravtsov, A.V., Valenzuela, O. & Prada, F. 1999 astro/ph 9901240

Kurucz, R.L. 1992, Rev. Mexicana Astron. Astrofis., 23, 181

Landoldt, A. 1992, AJ, 104, 340

Laird, J.B., Carney, B.W. & Latham, D.W. 1988, AJ, 95, 1843

Lynden-Bell, D. 1999, in "The Galactic Halo", ASP conf. series 165, ed. B. Gibson, T. Axelrod and M. Putnam

Lynden-Bell, D. & Lynden-Bell, R.M. 1995, MNRAS, 275, 429

Majewski, S.R. 1992, ApJS, 78, 87

Majewski, S.R., Munn, J.A., & Hawley, S.L. 1994, ApJ, 427, L37

Mateo, M.L. 1998 ARAA 36, 435

Mendez, R.A., Platais, I., Girard, T.M., Kozhurina-Platais, V., van Altena, W.F. 1999, ApJ, in press.

Morrison, H.L. 1993, AJ, 106, 578

Morrison, H.L., Flynn, C. & Freeman, K.C. 1990, AJ, 100, 1191

Morrison, H.L., Mateo, M., Olszewski, E.W., Harding, P., Dohm-Palmer, R., Freeman, K.C., & Norris, J.E. 2000, in preparation

Norris, J.E. and Hawkins, M.R.S. 1991, ApJ, 380, 104

Olszewski, E.W., Harding, P., Mateo, M.L., Morrison, H.L., Freeman, K.C. & Norris, J. 1999, in preparation

Paltoglou, G. & Bell, R.A. 1994 MNRAS, 268, 793

Pier, J. R. 1982, AJ, 87, 1515

Pier, J.R. 1983, ApJS, 52, 791

Pier, J. R. 1984, ApJ, 281, 260

Peterson, R.C. 1981, ApJ, 244, 989

Preston, G.W., Beers, T.C. & Shectman, S.A. 1994, AJ, 108, 538

Preston, G.W., Shectman, S.A., and Beers, T.C. 1991, ApJ, 375, 121

Ratnatunga, K.U. & Freeman, K.C. 1989, ApJ, 339, 126

Reid, N., & Majewski, S.R. 1993, pJ, 409, 635

Ryan, S.G. and Norris, J.E. 1991, AJ, 101, 1835

Saha, A. 1985, ApJ, 289, 310

Sandage, A. & Katem, B. 1964, ApJ, 139, 1088

Sandage, A., Katem, B. & Johnson, H.L. 1977, AJ, 82, 389

Sandage, A. & Fouts, G. 1987, AJ, 93, 74

Sandage, A. & Luyten, W.J. 1969, ApJ, 155, 913

Sandquist, E.L., Bolte, M., Langer, G.E., Hesser, J.E & Mendes de Olivera, C 1999, ApJ, 518, 262

Seitter, W.C. 1970, Atlas for Objective Prism Spectra, Bonner Spektral Atlas I, Ferd. Dummlers Verlag, Bonn

Schlegel, D.J., Finkbeiner, D.P. & Davis, M. 1998, ApJ, 500, 525

Searle, L. & Zinn, R. 1978, ApJ, 225, 357

Sommer-Larsen, J. & Christensen, P.R. 1985, MNRAS, 212, 851

Suntzeff, N.B., Kinman, T.D. and Kraft, R.P. 1991, ApJ, 367, 528

Totten, E.J. & Irwin, M.J. 1998, MNRAS, 294, 1

Twarog, B.A. & Anthony-Twarog, B.J. 1995, AJ, 109, 2828

Unavane, M., Wyse, R.F.G. & Gilmore, G. 1996, MNRAS, 278, 727

van Altena, W.M.F., Lee, J. & Hoffleit, E. 1991, The General Catalog of Trigonometric Parallaxes, a Preliminary Version (Yale University Observatory, New Haven)

Wetterer, C.J. & McGraw, J.T. 1996, AJ, 112, 1046

Wyse, R.F.G. & Gilmore, G. 1989, Comments in Astrophys., 13, 135

Zinn, R.J. 1985, ApJ, 293, 424

Zinn, R.J., 1993, in *The Globular Cluster- Galaxy Connection,* ASP Conf Series 48, edited by G. H. Smith & J. P. Brodie, (ASP, San Francisco), p. 38

This preprint was prepared with the AAS LaTeX macros v5.0.

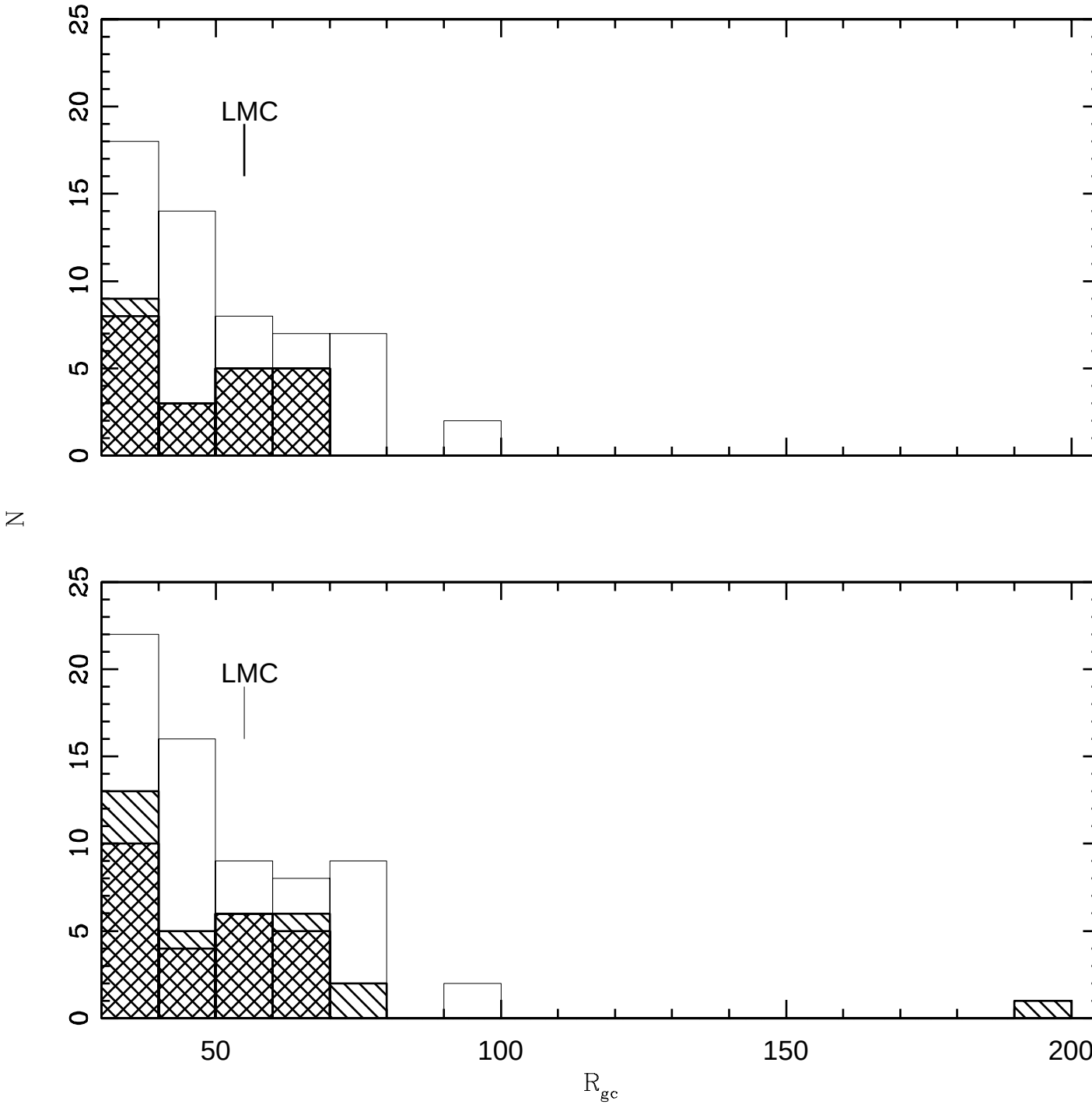

Fig. 1.— (a) Histogram of galactocentric distances to halo field stars with $R_{gc} > 30$ kpc known to date. Horizontal branch stars (RR Lyrae variables and BHB stars) are shown cross-hatched, red giants shaded and carbon stars comprise the rest. References for sources are given in Table 1. (b) Histogram of distances to outer halo field stars with the red giants and BHB stars of Olszewski et al. (1999) added – these stars were all confirmed spectroscopically during a single KPNO 4m run. The giant at 190 kpc needs a confirming spectrum with higher S/N before we can be 100% confident of its luminosity.

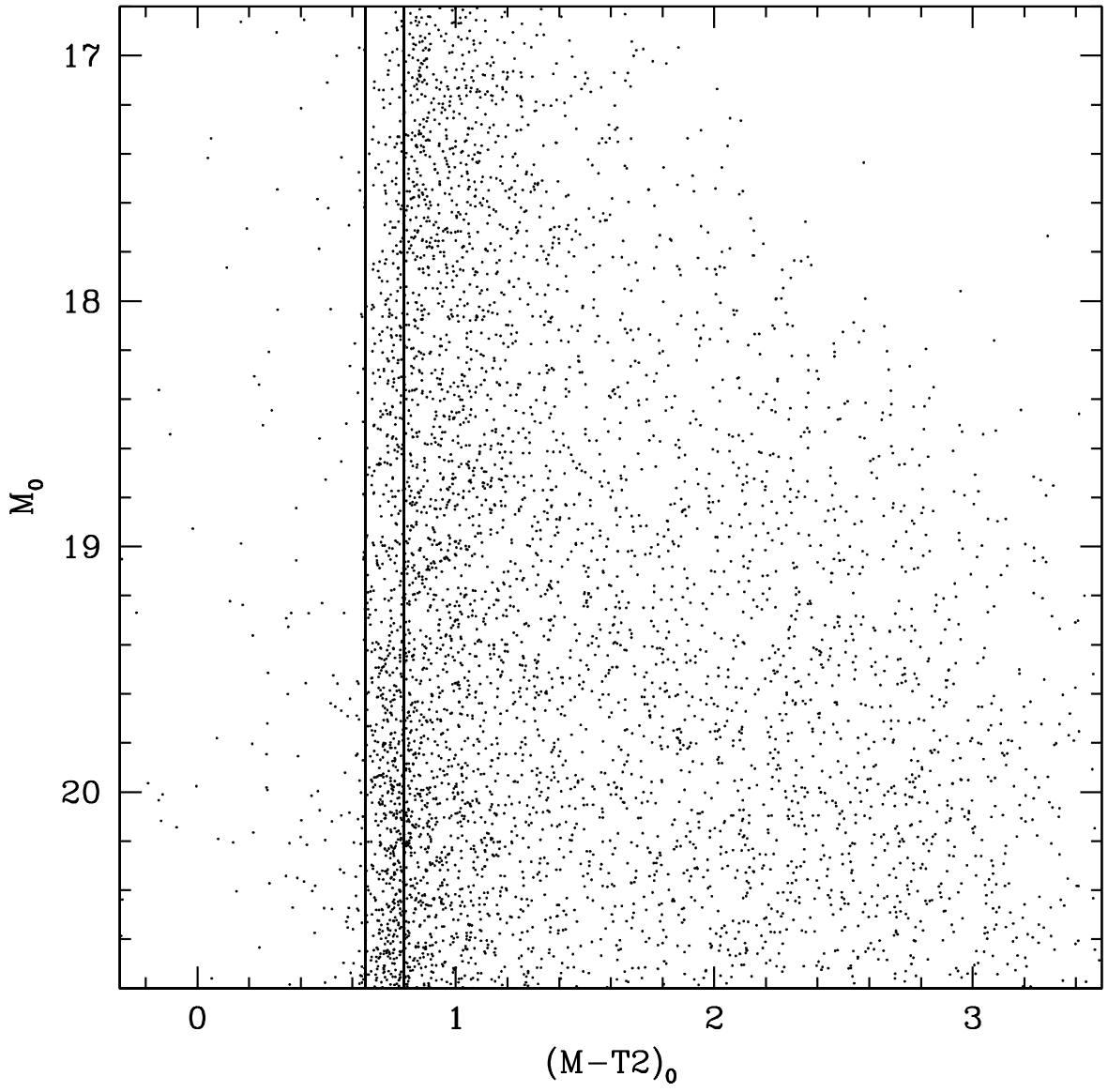

Fig. 2.— Color-magnitude diagram (M–T_2 vs M) for BTC fields of area 2.75 deg^2. Halo and thick disk turnoffs are marked: the halo turnoff is the bluer one, at $(M-T2)_0$=0.64.

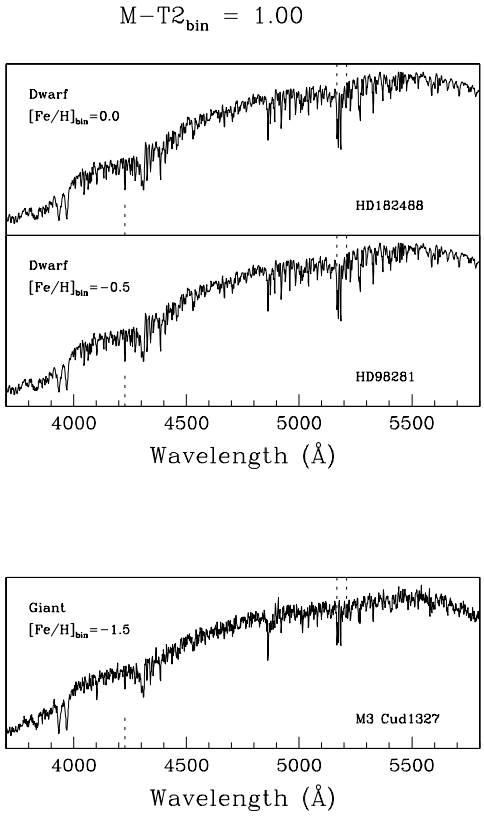

Fig. 3.— Spectra of known late-type giants and dwarfs taken on the KPNO 4m RC spectrograph in May 1999. Metallicity and $M-T_2$ color of star is given on each spectrum. Stars are ranked horizontally by M–T_2 color, with the bluest stars to the left, and by both luminosity and metallicity vertically. Dwarf spectra are shown at the top of each vertical panel and giants at the bottom, with the most metal-rich in each class at the top. The dwarfs in the bluer color range show a weak MgH feature because they are hotter than the temperatures where the MgH band is strongest. For stars with $M-T_2$ greater than 1.10, it can be seen that even metal-poor dwarfs have a strong MgH feature, and can easily be distinguished from metal-poor giants. MgH bandhead, the Mg b line at 5167Å and Ca I 4227Å line are marked.

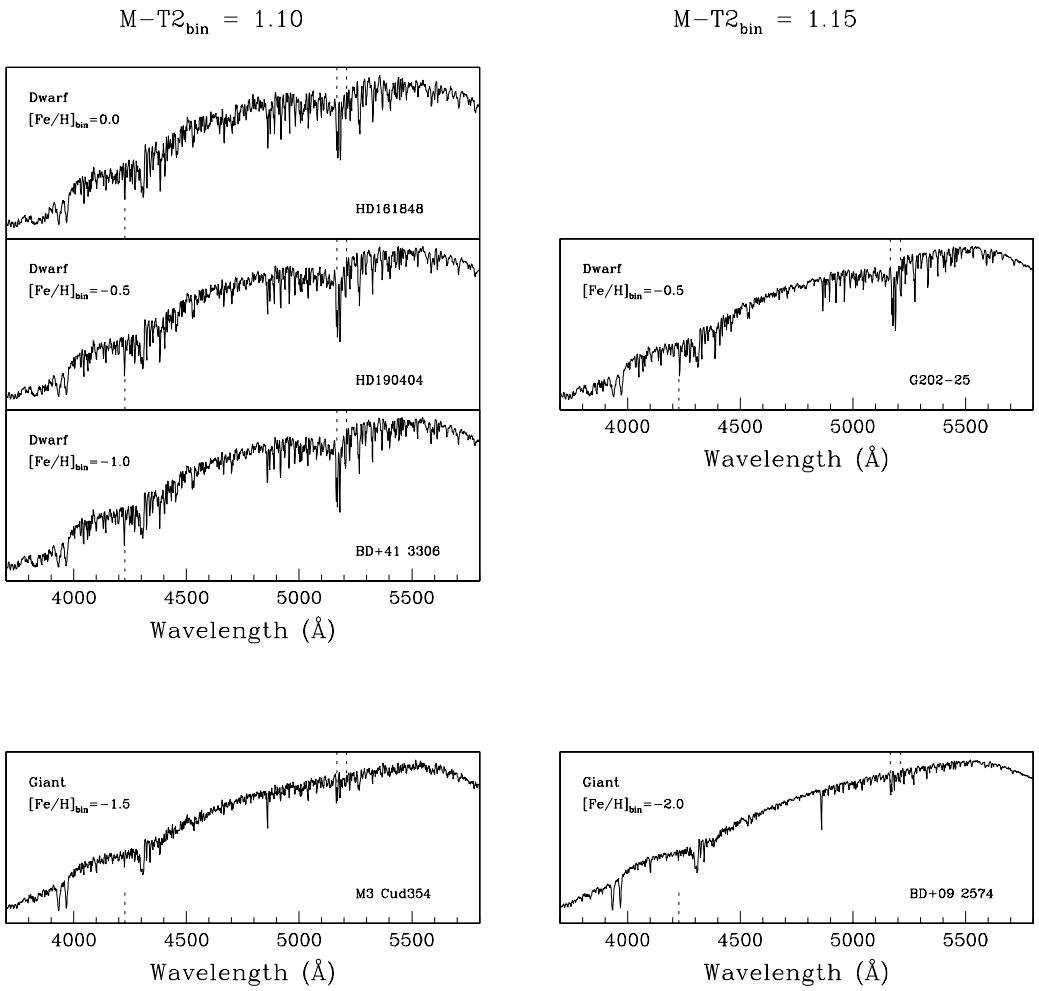
M−T2bin = 1.10
M−T2bin = 1.15
Dwarf
[Fe/H]bin=0.0
HD161848
Dwarf
[Fe/H]bin=−0.5
HD190404
Dwarf
[Fe/H]bin=−1.0
BD+41 3306
Dwarf
[Fe/H]bin=−0.5
G202−25
Giant
[Fe/H]bin=−1.5
M3 Cud354
Giant
[Fe/H]bin=−2.0
BD+09 2574
4000
4500
5000
5500
Wavelength (Å)

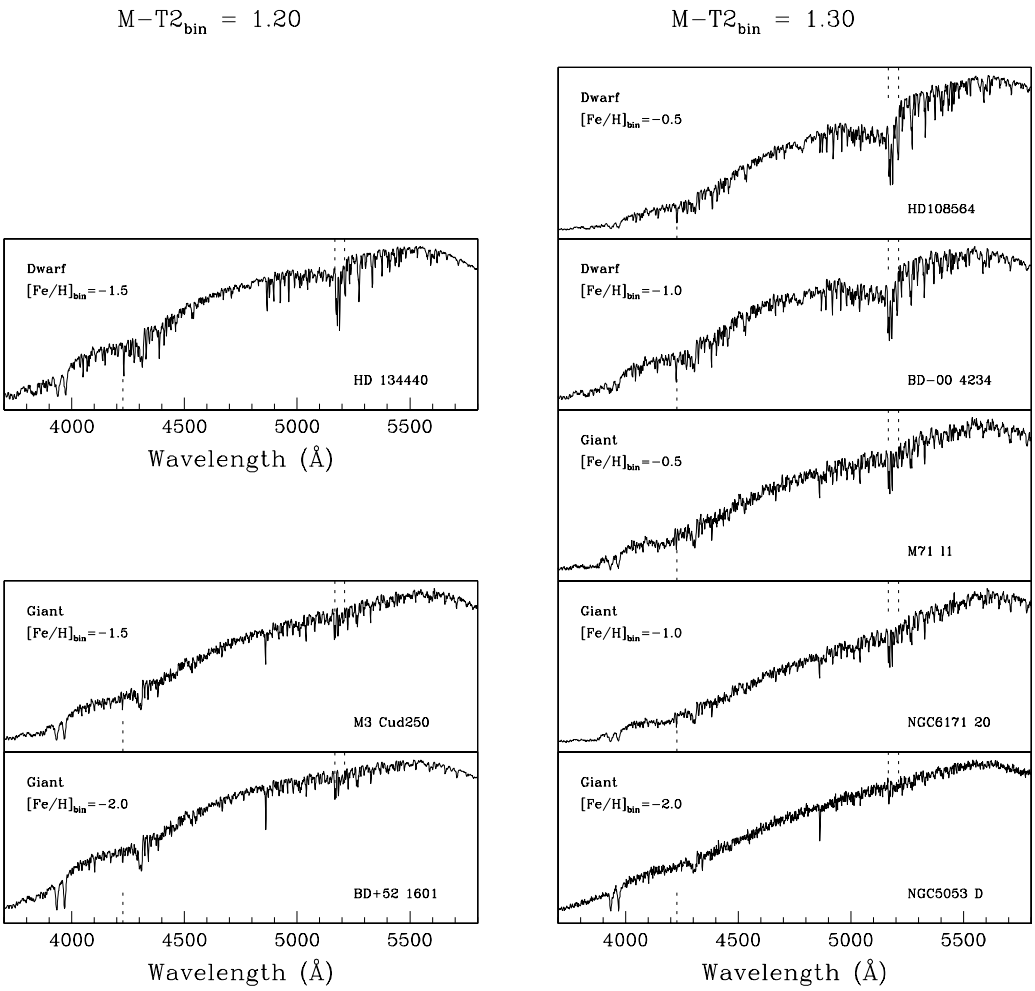
M−T2bin = 1.20
M−T2bin = 1.30
Dwarf
[Fe/H]bin=−1.5
HD 134440
Giant
[Fe/H]bin=−1.5
M3 Cud250
Giant
[Fe/H]bin=−2.0
BD+52 1601
Dwarf
[Fe/H]bin=−0.5
HD108564
Dwarf
[Fe/H]bin=−1.0
BD−00 4234
Giant
[Fe/H]bin=−0.5
M71 11
Giant
[Fe/H]bin=−1.0
NGC6171 20
Giant
[Fe/H]bin=−2.0
NGC5053 D
4000
4500
5000
5500
Wavelength (Å)

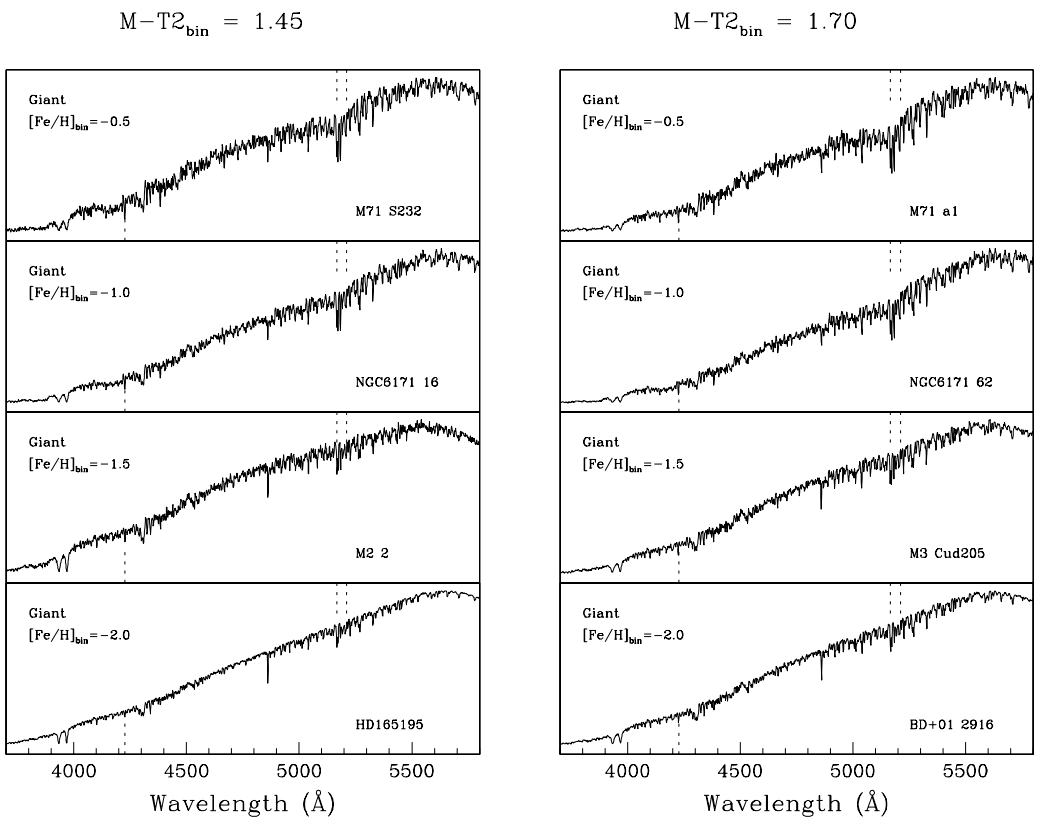
M−T2bin = 1.45
M−T2bin = 1.70
Giant
[Fe/H]bin=−0.5
M71 S232
Giant
[Fe/H]bin=−1.0
NGC6171 16
Giant
[Fe/H]bin=−1.5
M2 2
Giant
[Fe/H]bin=−2.0
HD165195
M71 a1
NGC6171 62
M3 Cud205
BD+01 2916
4000
4500
5000
5500
Wavelength (Å)

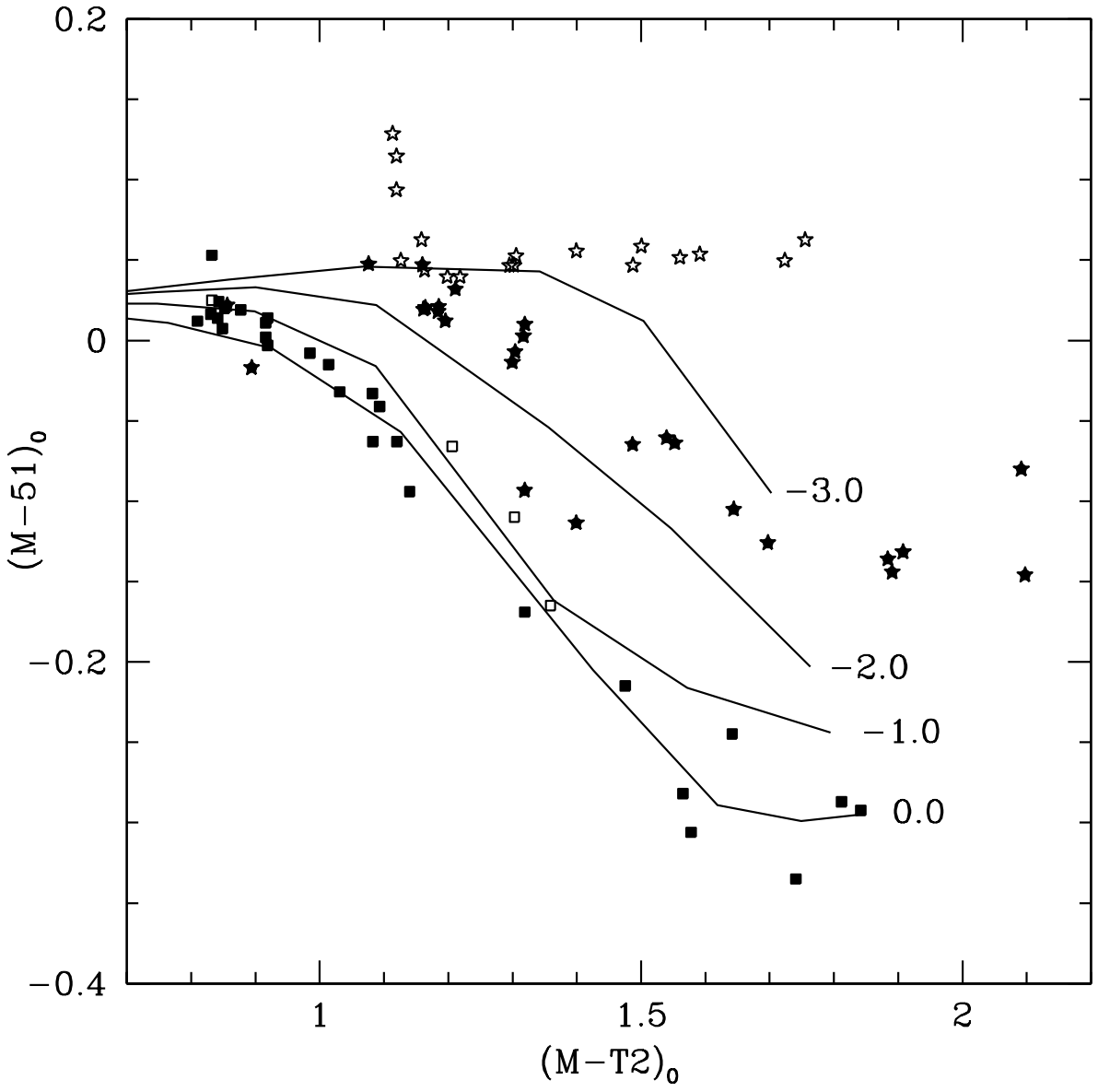

Fig. 4.— $M-51$ color for a selection of known late-type dwarfs and giants plotted versus $M-T_2$ color. Dwarfs with roughly solar metallicity are plotted as filled squares, those with [Fe/H] between –0.5 and –1.5 as open squares, solar abundance giants are plotted as closed stars, and metal-weak giants from the globular clusters NGC 6541 ([Fe/H] = –1.83, Zinn 1985) and NGC 6397 ([Fe/H] = –1.91, Zinn 1985) are plotted as open stars. Loci traced by the dwarf models of Paltoglou and Bell (1994) for [Fe/H] from 0.0 to –3.0 are also shown.

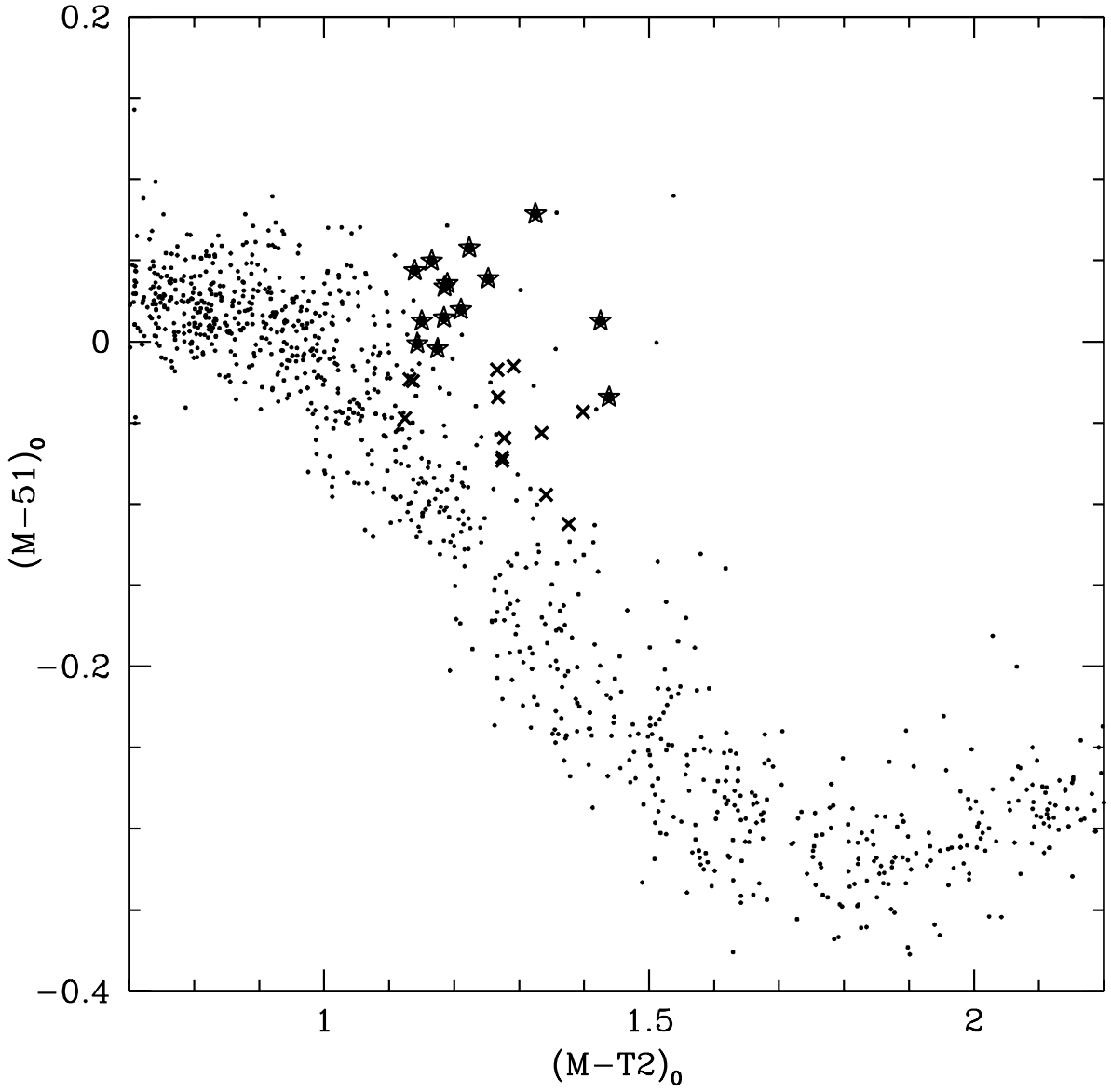

Fig. 5.— Spectroscopically confirmed halo giant stars in the $M-51$ versus $M-T_2$ diagram. Small circles are stars of all colors identified on several BTC fields, plotted to show the region where foreground dwarfs are found, crosses are halo giant candidates that were found to be dwarfs when spectra were obtained, and stars are spectroscopically confirmed halo giants. We deliberately observed stars with low $M-51$ values to delineate the dwarf region as accurately as possible.

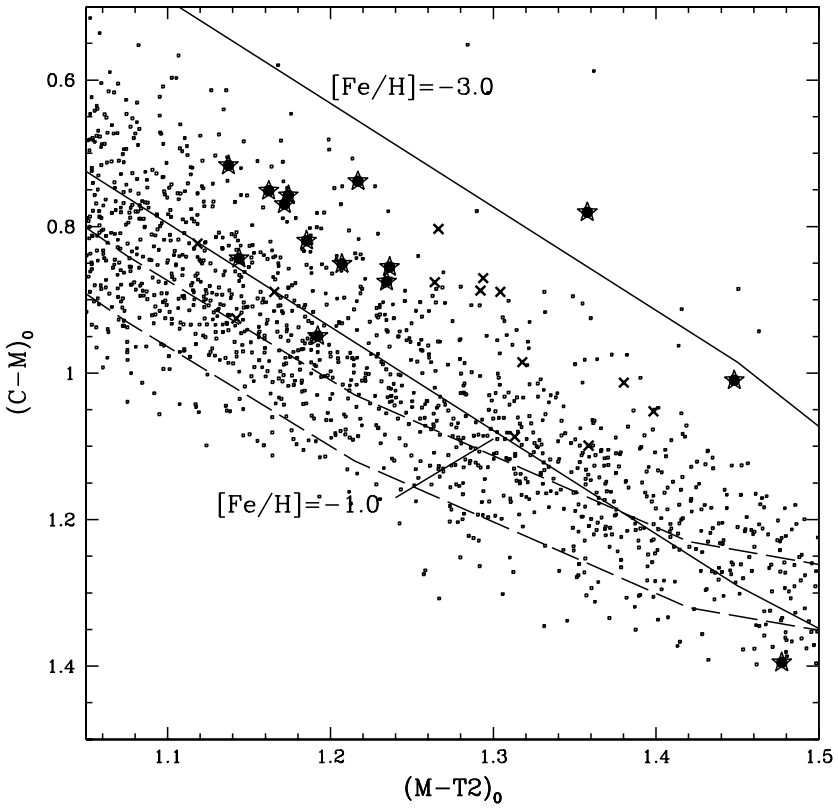

Fig. 6.— Spectroscopically confirmed halo giant stars in the $C-M$ versus $M-T_2$ diagram. Small circles are stars of all colors identified on 8 BTC fields, plotted to show the region where most foreground dwarfs are found, crosses are halo giant candidates that were found to be dwarfs when spectra were obtained, and stars are spectroscopically confirmed halo giants. Solid lines show the calibration lines for [Fe/H]=–1.0 and –3.0 from Geisler et al. (1991) and dashed lines show the calibration lines of Gonzalez and Piché (1992) for [Fe/H]=0.0 and –0.5. Since the metal-poor giants have a smaller separation from the dwarf sequences for cool stars, identification becomes less efficient there. It can be seen that the model prediction of roughly equal numbers of thick and thin disk dwarfs in our fields is borne out by our data: few stars are found below the [Fe/H]=0 line for dwarfs, and there are significant numbers of stars near the [Fe/H] =–0.5 line. [Fe/H]=–0.5 should represent the mean abundance for thick disk dwarfs.

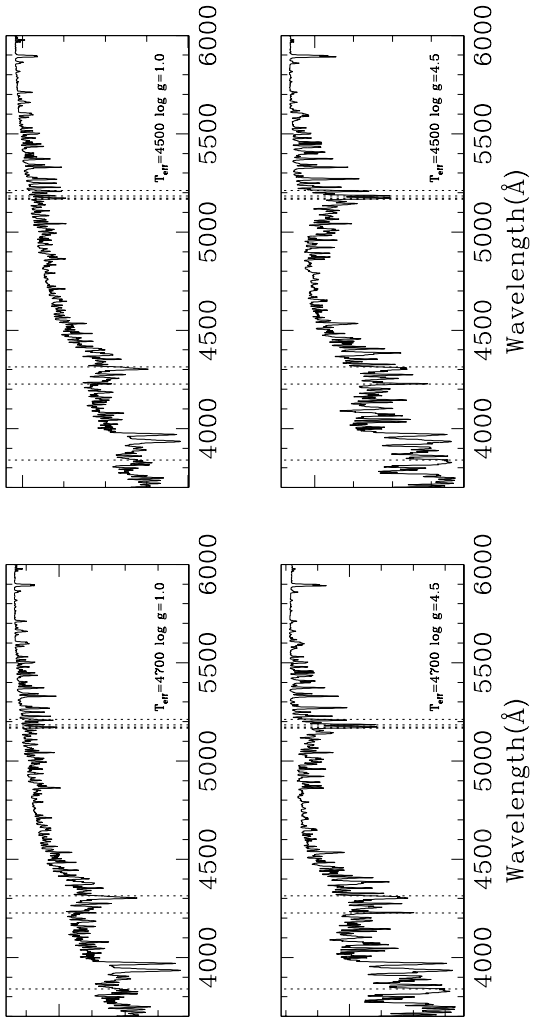

Fig. 7.— Model spectra for stars with [Fe/H] = –2.0, [α/Fe]=+0.4, log g = 1.0 and 4.5 and T_{eff}=4700 and 4500K. Positions of the MgH bandhead at 5211Å , the Mg triplet, the G band, the CaI 4227Å line and the group of FeI and MgI lines near 3840Å are marked.

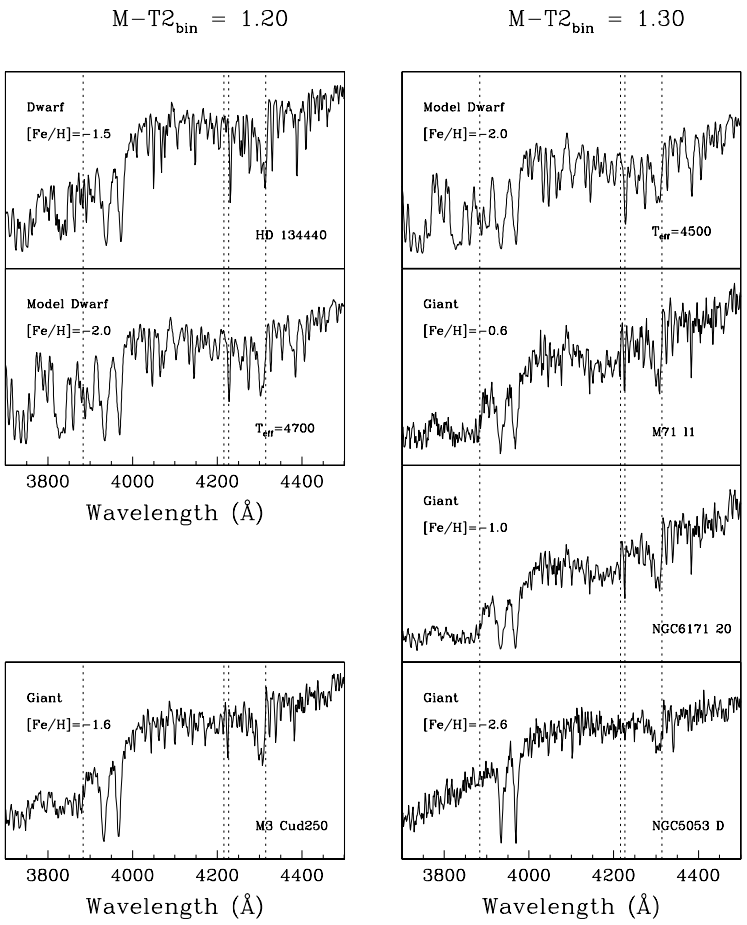

Fig. 8.— Spectra of metal-poor subdwarfs and giants of various metallicities, sorted into M–T_2bins, in the spectral region from 3700 to 4500Å . Wavelengths of the G band, Ca I 4227 line, blue CN bandhead and the UV CN bandhead are marked. HD 134440 has a radial velocity of 308 km/s, which explains why its spectral lines are offset from their rest wavelength.

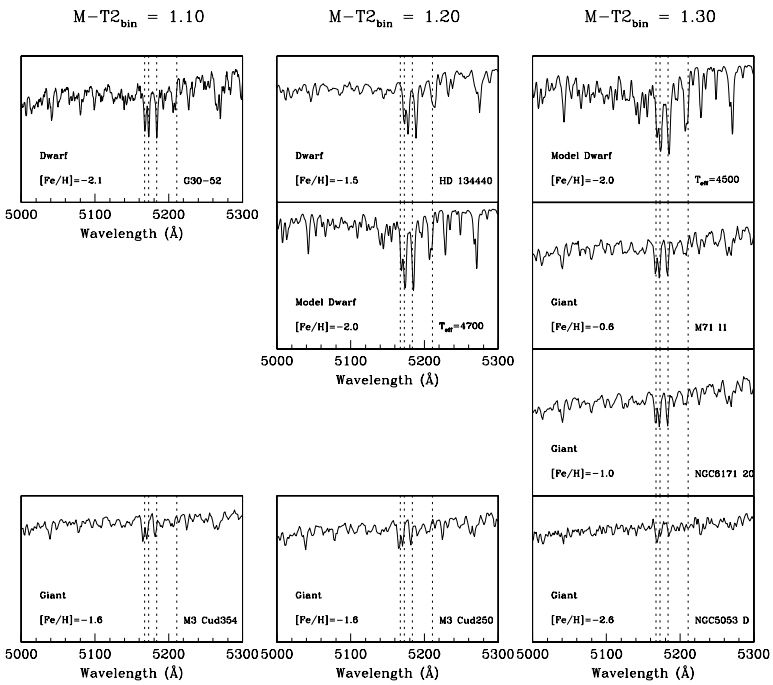

Fig. 9.— Spectra of metal-poor subdwarfs and giants of various metallicities, sorted into M–T_2bins, in the spectral region from 5000 to 5300Å . Wavelengths of the MgH bandhead at 5211Å and the Mg triplet are marked.

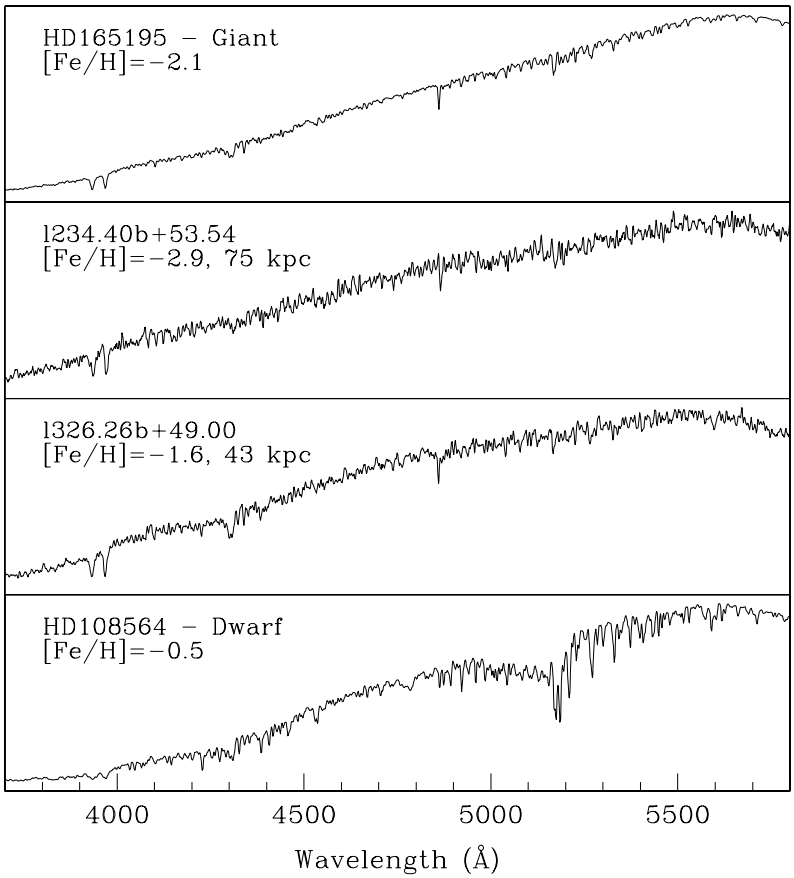

Fig. 10.— Spectra of two metal-poor red giants identified in our survey, compared with a known giant and dwarf. These spectra were obtained with the KPNO 4m RC spectrograph in May 1999 and will be described more fully in Olszewski et al. (1999). The star name gives its galactic longitude and latitude. The metallicity and distance of the star is given on each spectrum.

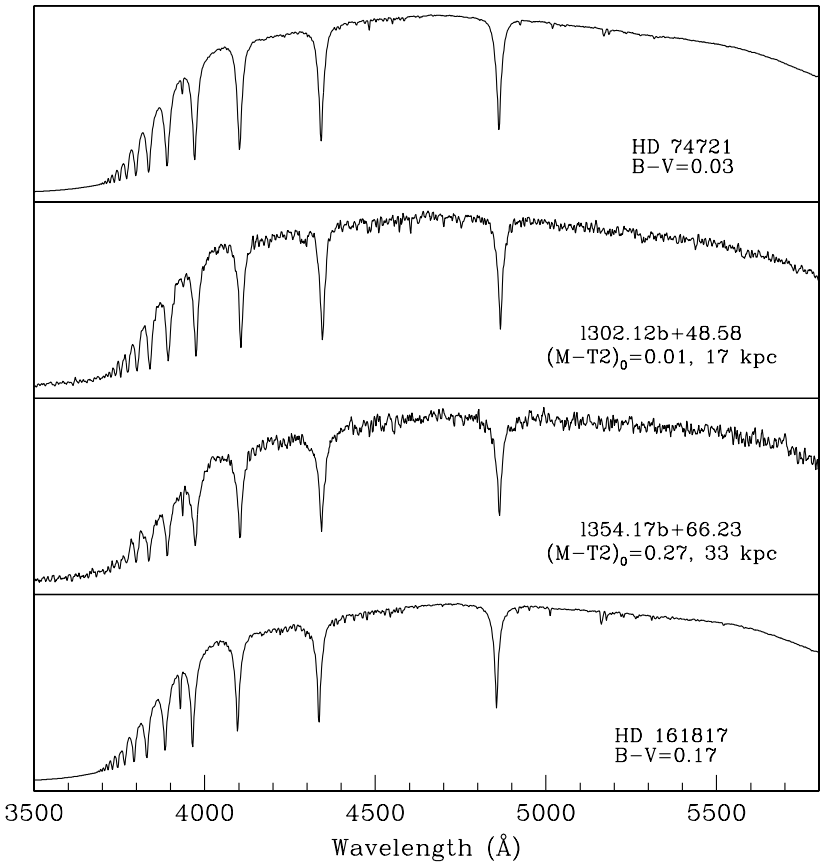

Fig. 11.— Spectra of BHB stars identified in our halo fields, compared with spectra of known field BHB stars. Stars are plotted in order of decreasing temperature. These data will be described more fully in Olszewski et al. (1999).

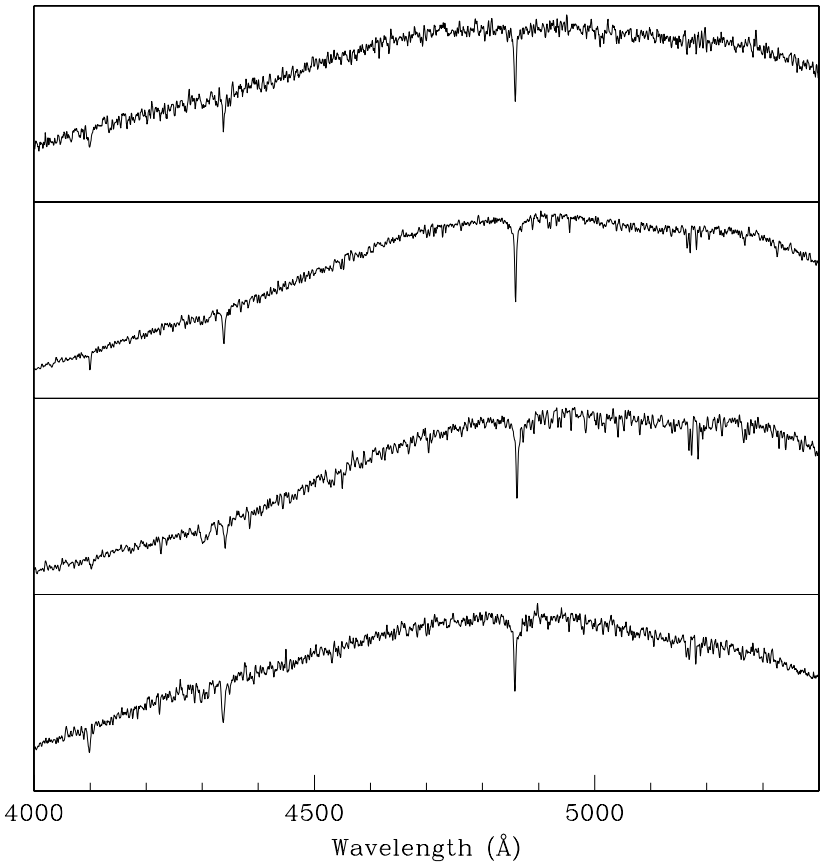

Fig. 12.— WIYN/Hydra spectra of main sequence turnoff stars identified in our halo fields.

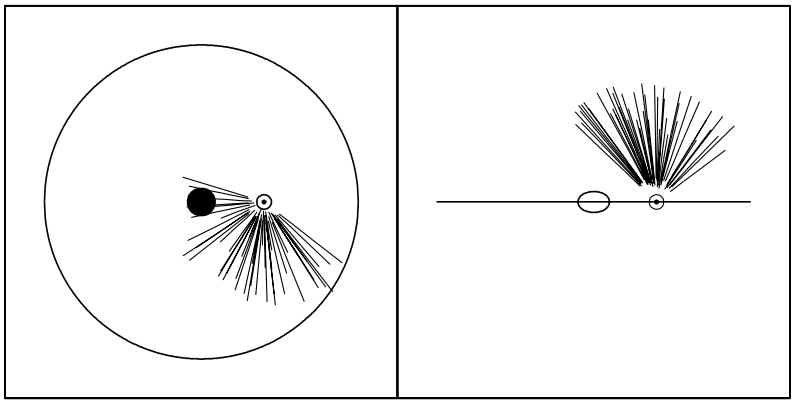

Fig. 13.— Face-on (left) and edge-on views of the Galaxy with the lines of sight traced by the 46 BTC fields shown. The position of the Sun, galactic center and edge of disk at R=20 kpc are shown.

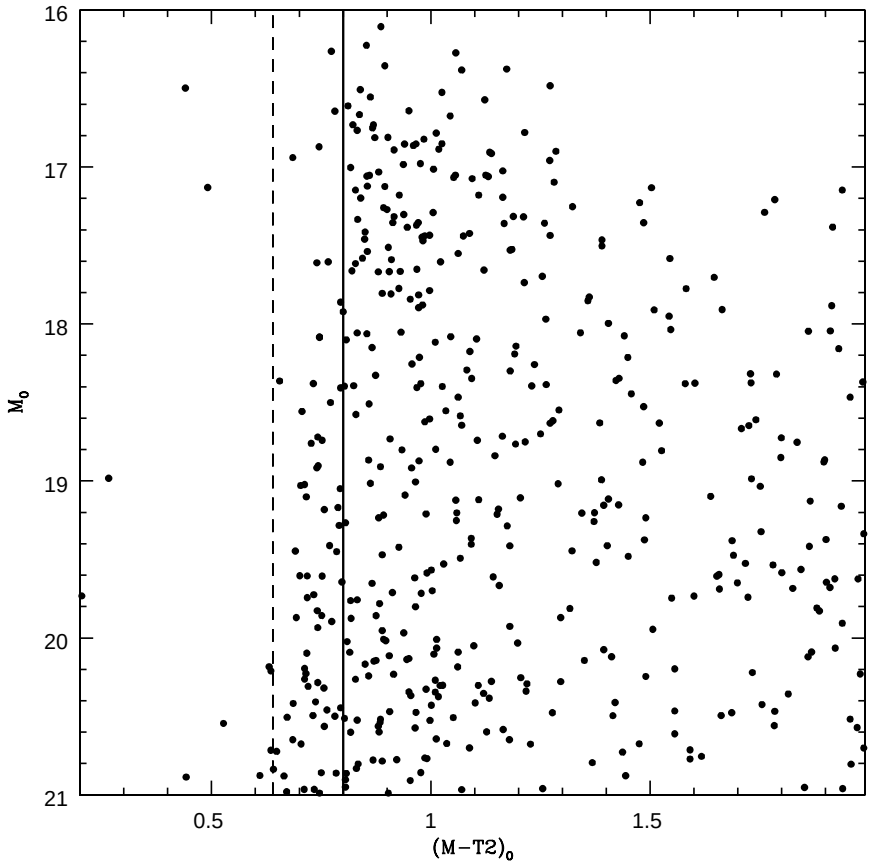

Fig. 14.— Color-magnitude diagram of a field at l=234, b=+32, with position of halo turnoff (dashed line) and thick disk turnoff (solid line) shown. The thick disk stars are clearly visible redward of the solid line for M brighter than 18. Halo turnoff stars are rare for these brightnesses and become increasingly common for fainter values of M.

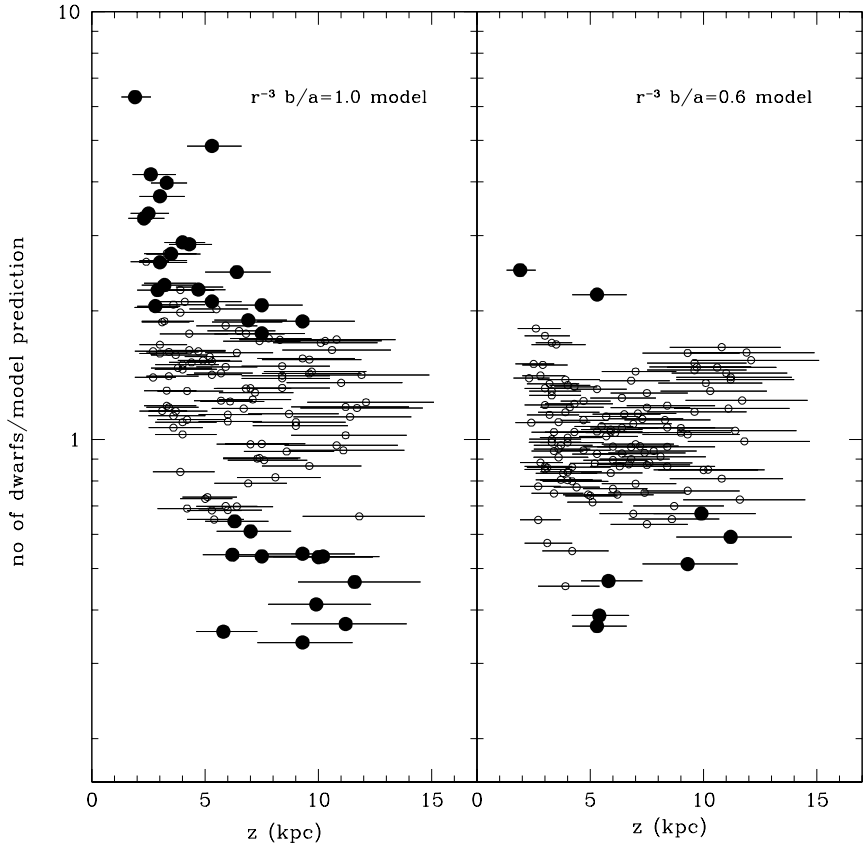

Fig. 15.— Ratio of number of turnoff stars to model prediction versus the range of z heights traversed. Points which are more than 2.5σ from the model are shown as solid symbols. The local halo density was adjusted to give the best fit for these fields: the spherical halo model uses a local density 40% of that given in Table 4 and the halo with b/a=0.6 has a local density 10% higher than that of Table 4.

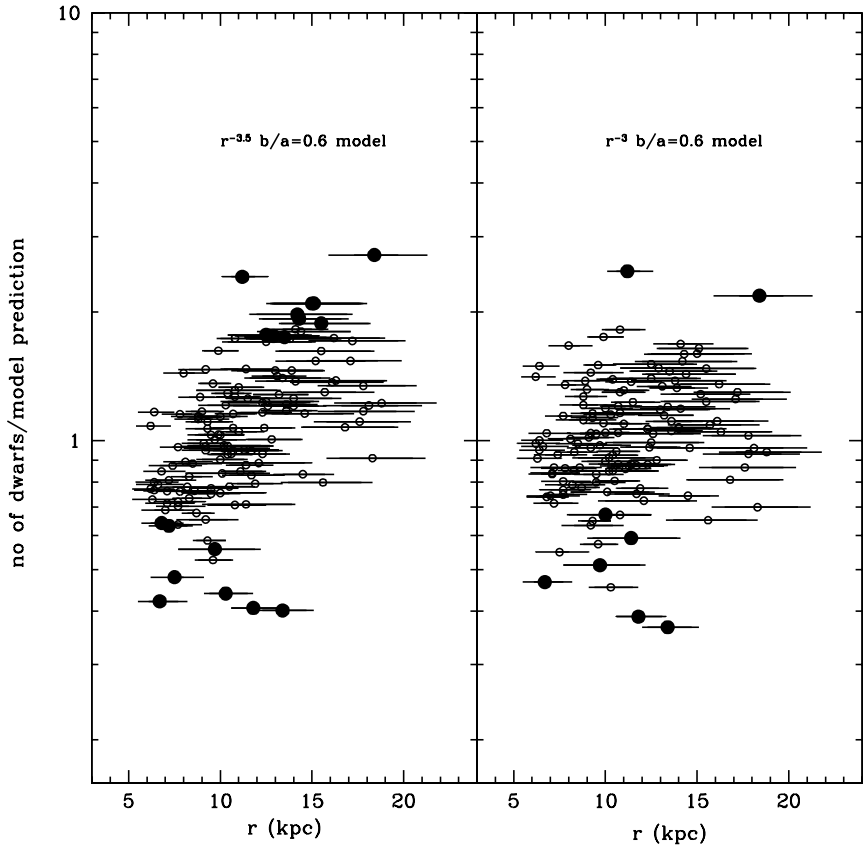

Fig. 16.— Ratio of number of turnoff stars to model prediction versus the range of R_{gc} values traversed by the line of sight. Points which are more than 2.5σ from the model are shown as solid symbols. The local halo density was adjusted to give the best fit for these fields: the model with exponent –3.5 uses a local density 40% larger than that given in Table 4 while the halo with exponent –3.0 has a local density 10% higher than that of Table 4.

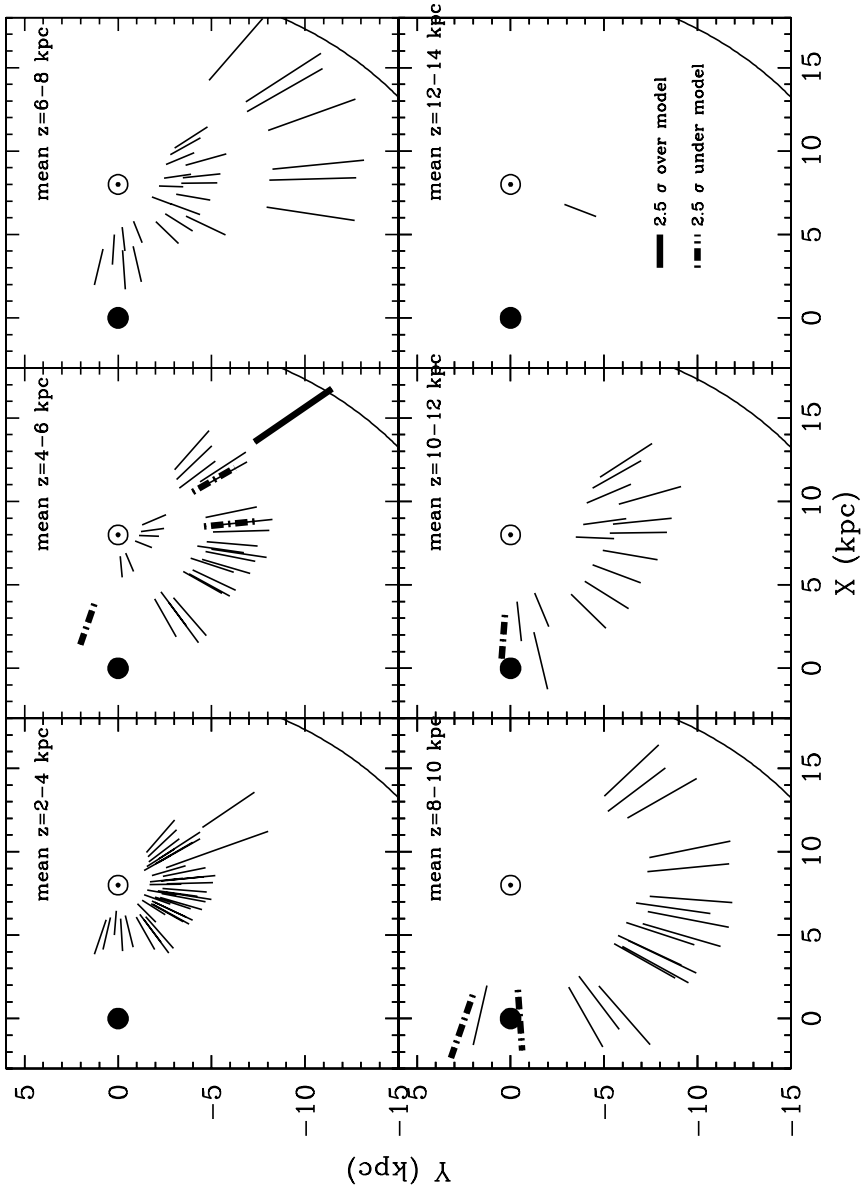

Fig. 17.— Face-on views of the galaxy for different ranges of z height. Lines of sight whose halo turnoff star numbers agree with our model are shown as solid lines. Lines of sight which are more than 2.5σ above the model are shown as bold lines, and those which are more than 2.5σ below are shown as dashed lines.

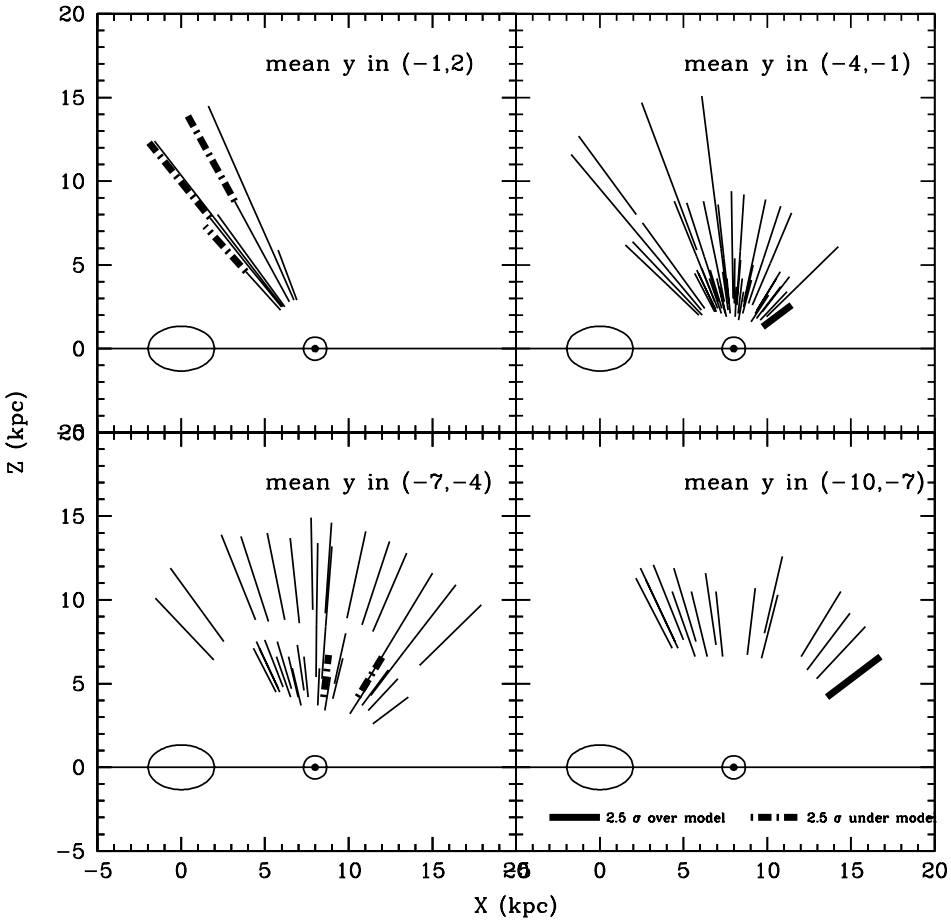

Fig. 18.— Edge-on view of the lines of sight of the 46 BTC fields. Symbols have the same meaning as in Fig.17.

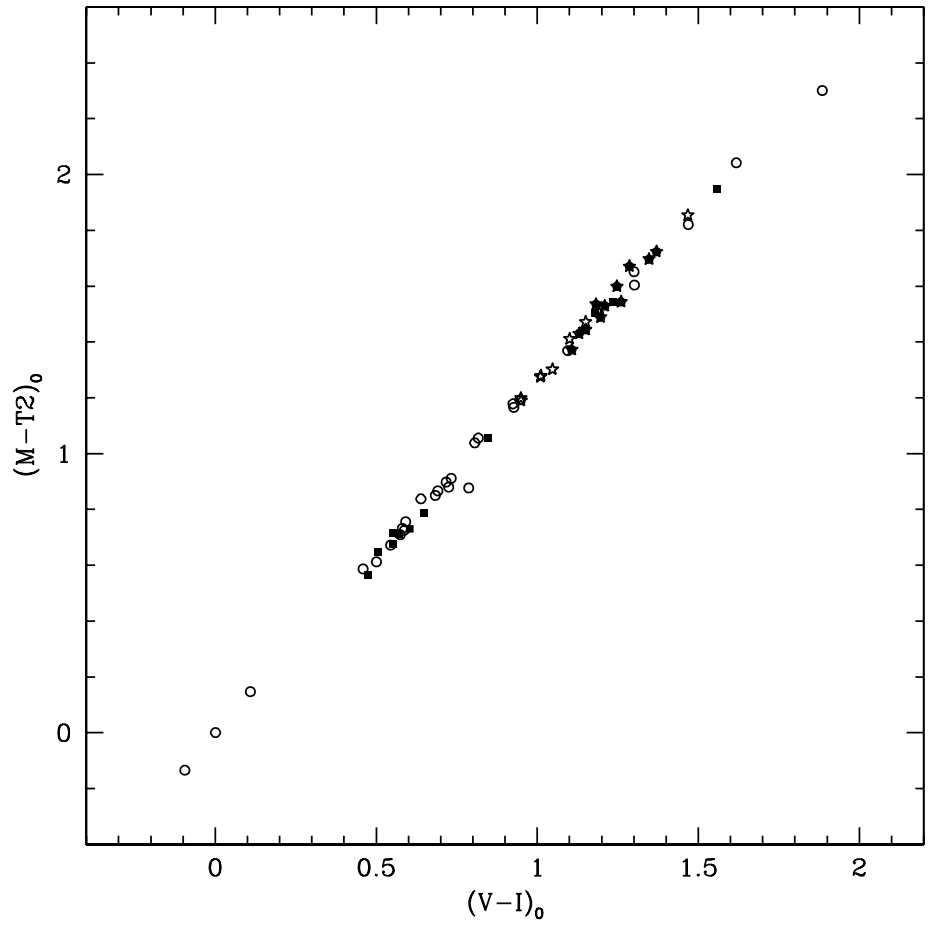

Fig. 19.— Relation between $M-T_2$ and $V-I$ for Landolt/Washington standards (giants plotted as stars, dwarfs as filled squares, unknown spectral types as open circles) and globular cluster giants (filled stars). It can be seen that there is a simple relation between Washington $M-T_2$ color and $V-I$ and that the relation does not depend on metallicity.

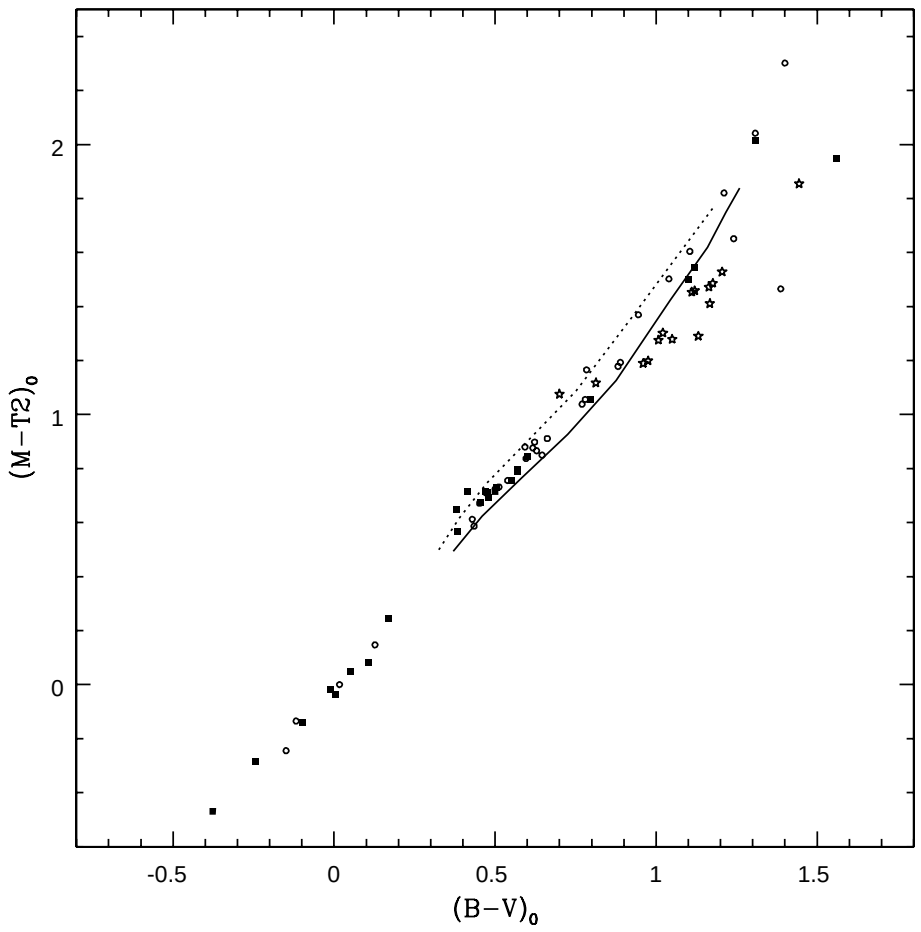

Fig. 20.— Relation between Washington $M-T_2$ and $B-V$ for Landolt/Washington standards (giants plotted as stars, dwarfs as filled squares, unknown spectral types as open circles)and dwarfs from Gonzalez and Piché (1992). The models of Paltoglou and Bell (1994) for solar abundance dwarfs (solid line) and [Fe/H] = –2.0 dwarfs (dotted line) are also shown.

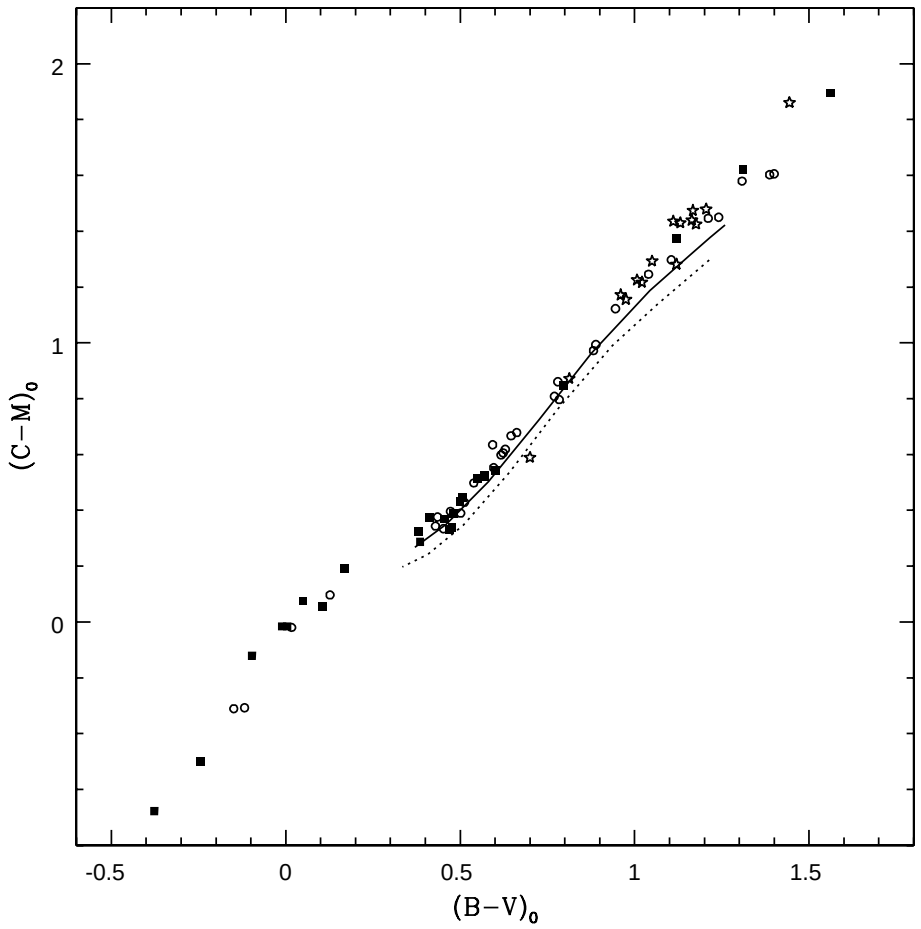

Fig. 21.— Relation between Washington $C-M$ and $B-V$ for Landolt/Washington standards (symbols as in Fig. 20) and dwarfs from Gonzalez and Piché (1992). Models for dwarfs of solar metallicity (solid line) and [Fe/H] = –2.0 (dotted line) from Paltoglou and Bell (1994) are also shown.

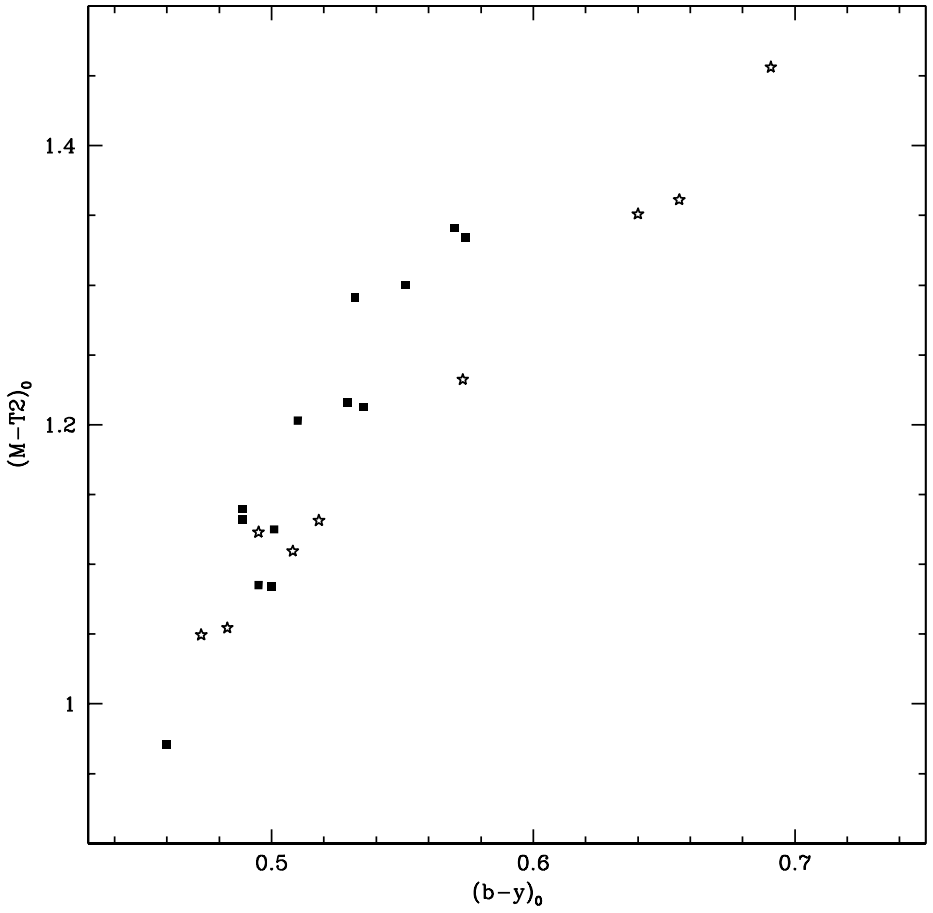

Fig. 22.— Relation between Washington $M-T_2$and Stromgren $b-y$ for giants and dwarfs (symbols as in Fig. 20).

Table 1. Literature Sources for Fig 1

Star type	References
RR Lyrae	Hawkins (1984)
	Ciardullo et al. (1989)
	Suntzeff et al. (1991)
	Wetterer and McGraw (1996)
BHB	Norris & Hawkins (1991)
	Flynn et al. (1995)
	Olszewski et al. (1999)
Red giant	Ratnatunga and Freeman (1989)
	Croswell et al. (1991)
	Olszewski et al. (1999)
Main sequence	Majewski (1992)
Carbon	Totten and Irwin (1998)

Table 2. Literature sources for metallicity and color for stars in Figs. 3

Star ID	[Fe/H]	$(b-y)_0$	$(B-V)_0$	$(V-I)_0$	$(M-T_2)_0$	Source
HD 98281	–0.25	0.46	···	···	0.97[a]	Eggen (1998)
HD 108564	–0.52	0.57	···	···	1.34[a]	Eggen (1998)
HD 134440	–1.52	···	···	0.973	1.22[b]	Peterson (1981); Bessell (1990)
HD 161848	–0.18	0.49	···	···	1.12[a]	Eggen (1998)
HD 165195	–2.1	0.73	···	···	1.53[a]	Bond (1980)
HD 182488	0.08	0.48	···	···	1.07[a]	Eggen (1998)
HD 190404	–0.44	···	···	···	1.114	Geisler (1984); Eggen (1998)
BD+52 1601	–1.8	0.55	···	···	1.18[a]	Bond (1980)
BD+41 3306	–0.87	···	0.81	···	1.10:	Peterson (1981); Carney (1979)
BD+09 2574	–2.4	0.54	···	···	1.17[a]	Bond (1980); Twarog and Anthony-Twarog (1995)
BD+01 2916	–2.0	···	···	···	1.68	Bond (1980); Geisler (1986)
BD−00 4234	–0.99	0.58	···	···	1.36[a]	Peterson (1981); Twarog and Anthony-Twarog (1995)
G202-25	–0.38	···	0.87	···	1.15:	Laird et al. (1988)
NGC 5053 D	–2.58	···	1.01	···	1.3:	Zinn (1985); Sandage et al. (1977)
M3 Cud205	–1.66	···	1.36	···	1.75:	Zinn (1985); Cudworth (1979)
M3 Cud250	–1.66	···	0.94	···	1.20:	
M3 Cud354	–1.66	···	0.82	···	1.10:	
M3 Cud1327	–1.66	···	0.74	···	1.0:	
NGC 6171 16	–0.99	···	1.11	···	1.45:	Zinn (1985); Sandage and Katem (1964)
NGC 6171 20	–0.99	···	1.06	···	1.3:	
NGC 6171 62	–0.99	···	1.29	···	1.7:	
M71 a1	–0.58	···	1.30	···	1.7:	Zinn (1985); Cudworth (1985)
M71 l1	–0.58	···	0.99	···	1.3:	
M71 s232	–0.58	···	1.18	···	1.5:	
M2 2	–1.62	···	···	1.20	1.50	Zinn (1985); Armandroff and Da Costa (1991)

[a]These values of $M-T_2$were derived from $b-y$.

[b]These values of $M-T_2$were derived from $V-I$.

[:]These values of $M-T_2$were derived from $B-V$and are likely to be less accurate than those derived from $b-y$or $V-I$.

Table 3. Turnoff colors for Globular Clusters

Cluster	$(b-y)_0$	$(V-I)_0$	References
M92	···	0.531	Johnson and Bolte (1998)
NGC 7099	···	0.485	Sandquist et al. (1999)
NGC 6397	0.294	···	Anthony-Twarog et al. (1992)
47 Tucanae	···	0.70	Kaluzny et al. (1998)

Table 4. Halo turnoff star luminosity function for stars with $B-V$ between 0.38 and 0.50

M_V	Φ (stars per kpc^3)	Number of stars in CLL sample
3.5	73.1	2
4.0	986.0	13
4.5	2695.7	46
5.0	807.8	17
5.5	151.2	5